J Neurophysiol 90: 2660–2675, 2003.
First published June 18, 2003; 10.1152/jn.00751.2002.

Spectrotemporal Structure of Receptive Fields in Areas AI and AAF of Mouse Auditory Cortex

Jennifer F. Linden,[1,2] Robert C. Liu,[1,3,4] Maneesh Sahani,[1,2,5] Christoph E. Schreiner,[1,2,4] and Michael M. Merzenich[1,2,4]

[1]*Keck Center for Integrative Neuroscience, Departments of* [2]*Otolaryngology and* [3]*Physiology, and* [4]*Sloan-Swartz Center for Theoretical Neurobiology, University of California, San Francisco, California 94143; and* [5]*Gatsby Computational Neuroscience Unit, University College, London, WC1N 3AR, United Kingdom*

Submitted 3 September 2002; accepted in final form 13 June 2003

Linden, Jennifer F., Robert C. Liu, Maneesh Sahani, Christoph E. Schreiner, and Michael M. Merzenich. Spectrotemporal structure of receptive fields in areas AI and AAF of mouse auditory cortex. *J Neurophysiol* 90: 2660–2675, 2003. First published June 18, 2003; 10.1152/jn.00751.2002. The mouse is a promising model system for auditory cortex research because of the powerful genetic tools available for manipulating its neural circuitry. Previous studies have identified two tonotopic auditory areas in the mouse—primary auditory cortex (AI) and anterior auditory field (AAF)—but auditory receptive fields in these areas have not yet been described. To establish a foundation for investigating auditory cortical circuitry and plasticity in the mouse, we characterized receptive-field structure in AI and AAF of anesthetized mice using spectrally complex and temporally dynamic stimuli as well as simple tonal stimuli. Spectrotemporal receptive fields (STRFs) were derived from extracellularly recorded responses to complex stimuli, and frequency-intensity tuning curves were constructed from responses to simple tonal stimuli. Both analyses revealed temporal differences between AI and AAF responses: peak latencies and receptive-field durations for STRFs and first-spike latencies for responses to tone bursts were significantly longer in AI than in AAF. Spectral properties of AI and AAF receptive fields were more similar, although STRF bandwidths were slightly broader in AI than in AAF. Finally, in both AI and AAF, a substantial minority of STRFs were spectrotemporally inseparable. The spectrotemporal interaction typically appeared in the form of clearly disjoint excitatory and inhibitory subfields or an obvious spectrotemporal slant in the STRF. These data provide the first detailed description of auditory receptive fields in the mouse and suggest that although neurons in areas AI and AAF share many response characteristics, area AAF may be specialized for faster temporal processing.

INTRODUCTION

The mouse holds great potential as a model system for studies of auditory cortical processing and plasticity for three reasons. First, mouse studies can benefit from powerful genetic engineering technologies. For example, inducible cell-specific knockout techniques (e.g., McHugh et al. 1996; Nirenberg and Cepko 1993) could be used to deduce the roles of different cortical cell types in auditory perception and learning, and mouse models of human diseases (e.g., Battey 2001; Henry and McGinn 1992) could be used to examine the cortical causes and consequences of auditory pathologies. Second, mice rely heavily on audition for communication (Haack et al. 1983; Nyby 2001), discriminating between a variety of behaviorally significant and acoustically distinct vocalizations (Ehret 1992; Ehret and Riecke 2002; Geissler and Ehret 2002). Third, mouse auditory genetics, anatomy, and subcortical physiology have already been well characterized (for a review, see Willott 2001).

Previous studies have distinguished at least five auditory fields in mouse cortex (Stiebler et al. 1997) on the basis of tonotopy, spontaneous activity, and general characteristics of responses to tones, noise bursts, and frequency sweeps. These fields include the primary auditory field (AI), the anterior auditory field (AAF), the ultrasonic field (UF, which may be a continuation of AI and/or AAF into ultrasonic frequency sensitivities) (Hofstetter and Ehret 1992), and two higher-order auditory areas, the secondary auditory field (AII) and the dorsoposterior field (DP). The two tonotopic areas AI and AAF appear to be organized as in other mammals with a reversal of tonotopy across the high-frequency border between the two fields. However, except for one very brief report (Shen et al. 1999), there is no published data on the structure of auditory receptive fields in these areas. Better descriptions of auditory receptive field structure in mouse AI and AAF are a prerequisite for understanding cortical processing of auditory information in the mouse.

With that goal in mind, we here describe the auditory receptive fields of neurons recorded extracellularly in thalamorecipient layers of mouse AI and AAF. At each recording site, we employed two different response characterization strategies. Conventional frequency-intensity tuning curves and poststimulus time histograms (PSTHs) were determined from multiunit responses to isolated tone bursts to identify auditory fields and to assess the properties of multiunit activity at each site in a manner consistent with many previous studies of auditory cortex responses in other species. Then spectrotemporal receptive fields (STRFs) were estimated from single-unit or unit-cluster responses to dynamic random chord stimuli at the same recording sites, to characterize the receptive fields of single neurons or small numbers of neurons in greater spectrotemporal detail. Similar spectrographic reverse-correlation methods have previously been used to characterize STRFs in

Address for reprint requests and other correspondence: J. F. Linden, University of California, San Francisco, Box 0732, 513 Parnassus Ave., San Francisco, CA 94143-0732 (E-mail: linden@phy.ucsf.edu).

The costs of publication of this article were defrayed in part by the payment of page charges. The article must therefore be hereby marked "*advertisement*" in accordance with 18 U.S.C. Section 1734 solely to indicate this fact.

the auditory cortex of the guinea pig (Rutkowski et al. 2002), cat (Miller et al. 2001, 2002; Schnupp et al. 2001), ferret (Depireux et al. 2001; Kowalski et al. 1996a), and monkey (deCharms et al. 1998) and also to describe the properties of auditory neurons in other brain areas and other species (e.g., Eggermont et al. 1983a; Escabi and Schreiner 2002; Keller and Takahashi 2000; Qiu et al. 2003; Sen et al. 2001; Theunissen et al. 2000; for a review, see Eggermont et al. 1983b).

These complementary analyses provide a detailed picture of the spectral, temporal, and spectrotemporal properties of neuronal responses in mouse auditory cortex. They reveal that several features of mouse auditory responses are common to both areas AI and AAF, including very short minimum response latencies, broad spectral tuning, and, for nearly one-quarter of the neurons, significant spectrotemporal inseparability (i.e., interaction between spectral and temporal sensitivities). Areas AI and AAF differ, however, in the distributions of both first-spike latencies and peak latencies and the durations of responses and of receptive fields. These results are consistent with findings from similar studies in other species and suggest that although neurons in areas AI and AAF share many response characteristics, AAF may be specialized for processing faster temporal modulations. This detailed characterization of mouse auditory receptive fields now provides a foundation for future studies of auditory cortical processing and plasticity in mice.

METHODS

Animals

Twelve adult CBA/CaJ mice (6–15 wk old) were used in this study. The CBA/CaJ strain was chosen because mice of this inbred strain have excellent hearing with minimal age-related hearing loss (Zheng et al. 1999) and are often used as a standard in studies of mouse auditory physiology and behavior (e.g., Willott et al. 1993, 2000).

Surgical procedures

All surgical procedures conformed to protocols approved by the University of California at San Francisco's Committee on Animal Research and were in accordance with federal guidelines for care and use of animals in research. Mice were anesthetized and maintained at a surgical plane of anesthesia with ketamine and medetomidine. Dexamethasone was administered to control edema, atropine or glycopyrrolate to minimize respiratory secretions, and Ringer solution or saline to ensure adequate hydration. Heart rate, respiration rate, and temperature were monitored throughout each experiment; temperature was maintained near 37.5°C with a rectal probe and a homeothermic blanket system (Harvard Instruments). Tracheotomies were performed on some of the mice to allow for artificial respiration with a pressure-controlled ventilator (Kent Scientific).

Once anesthetized and prepared for surgery, each mouse was placed in a nose clamp to immobilize its head. Topical anesthetics were applied to the scalp, and the skin transected to expose the skull. A hand drill and scalpel were then used to remove a section of bone over the left auditory cortex. Silicone oil was applied to the dural surface to keep the exposed cortex moist, and electrode penetrations were made through the dura.

Recording procedures

All experiments were conducted in a sound-shielded anechoic chamber (Industrial Acoustics). Auditory stimuli were delivered from two free-field speakers (Dynaudio and Ultrasound Advice), one covering the low-frequency portion of the mouse hearing range and another covering the ultrasound range. Animals were positioned with the right ear near the opening of an acoustical horn (Ultrasound Advice) and a sound-attenuating plug in the left ear so that the free-field stimuli were presented monoaurally to the right ear. Acoustic calibration was performed before every experiment with a 1/4-in Bruel and Kjaer microphone placed at the opening of the acoustical horn so that the speaker output could be corrected to ensure a flat frequency response (±2 dB SPL) and <2% total harmonic distortion over the appropriate frequency range for each speaker.

Epoxylite-coated tungsten electrodes (1–4 MΩ impedance; Fred Haer and Co.) were introduced into the left auditory cortex in penetrations orthogonal to the cortical surface. Recordings targeted thalamorecipient layers III/IV (Smith and Populin 2001) by cortical depth (350–600 μm below the dural surface) and by the polarity and size of stimulus-evoked local field potentials. These criteria were previously validated in separate histological studies (data not shown). Neuronal responses to noise bursts, frequency sweeps, and repeated tone bursts were then examined to determine the location of each recording in the mouse auditory cortex map (Fig. 1), according to criteria described by Stiebler et al. (1997). Neurons in areas AI and AAF were identified by their nonadapting responses to repeated tone bursts at interstimulus intervals of 400–500 ms and by a reversal of tonotopy along the rostral-caudal axis. Neurons in area UF were distinguished by strong tuning to ultrasonic frequencies and sensitivity to frequency sweeps. Area AII was characterized by its fractured tonotopy and by strongly habituating neuronal responses to repeated tone bursts. Neurons in area DP were identified by their bursty spontaneous activity and persistent locking to repeated stimuli.

The auditory cortex was not mapped extensively in these experiments but only enough to identify the likely locations of AI and AAF. At recording sites judged to be in thalamorecipient layers of these two auditory fields, neuronal responses were then characterized in detail. This characterization proceeded in two stages. In the first stage, simple tonal stimuli (see following text) were presented with the intensity and frequency of the tone bursts varying pseudorandomly over either a low- or a high-frequency range. Because different speakers were required to cover the two frequency ranges—and because simultaneous playback from both speakers was not feasible for technical reasons—responses to tonal stimuli in each frequency range were recorded separately. Electrode signals were amplified (Axon Instruments), band-pass filtered between 300 and 6,000 Hz (Stewart) and then thresholded in software (Brainware, Tucker-Davis Technologies) to extract the times of neuronal action potentials. Thresholds were set above the level of noise in the recording but usually low enough to include spikes of varying amplitude; therefore the recorded responses to tonal stimuli typically represented multiunit activity.

In the second stage of the characterization, repeated trials of the dynamic random chord stimuli (see following text) were played

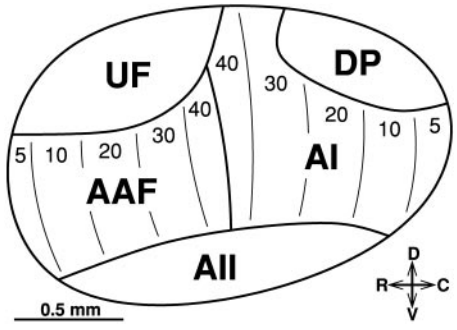

FIG. 1. Mouse auditory cortex. AI, primary auditory field; AAF, anterior auditory field; UF, ultrasonic field; AII, secondary auditory field; DP, dorsoposterior field. Note the reversal of tonotopy along the rostral-caudal axis between AI and AAF. Diagram adapted from Stiebler et al. (1997).

continuously for many minutes. Like the tonal stimuli, these complex stimuli spanned either a low- or a high-frequency range; the two types of stimuli were presented sequentially at each recording site (separated in time by at least a few minutes). Neuronal responses to dynamic random chord stimuli were recorded with minimal band-pass filtering (100–10,000 Hz), and the amplified electrode signals were sampled continuously (National Instruments) for further processing off-line. The recordings were later band-pass filtered in software (300–6,000 Hz, 5th-order Butterworth filters) and then analyzed using Bayesian spike-sorting techniques (Lewicki 1994) (user interface software by M. Kvale, UCSF) to extract responses from single units or small clusters of neurons. These single-unit or unit-cluster responses were used to estimate STRFs (see following text). Because multiple single units or distinct neuronal clusters could often be obtained from spike sorting of the continuous recordings, the total number of STRFs included in the analyses of responses to dynamic random chord stimuli differed from the number of recording sites included in analyses of responses to tonal stimuli.

Tonal stimuli

Tonal stimuli consisted of 60-ms tone bursts, ramped up and down with 5-ms cosine gates. The frequency and intensity of each tone burst varied pseudorandomly over the range of possible values in the stimulus set. Frequencies covered 2–32 kHz for the low-frequency stimulus set and 25–100 kHz for the high-frequency stimulus set, in 1/10-octave increments. Intensities ranged from 0 to 70 dB SPL in 5-dB increments. Each of the possible frequency-intensity combinations was presented only once per stimulus set. The time interval between successive tone bursts was $\geq$400 ms.

Analysis of responses to tonal stimuli

Spike times collected during presentation of tonal stimuli were analyzed off-line using interactive Matlab software (Ben Bonham, UCSF). The analysis proceeded as follows. First, rastergrams in which trials were grouped by tone frequency and/or by tone intensity were examined to identify a time window that appeared to encompass the maximal stimulus-evoked response. This time window, which was determined by eye based on the concentration of spikes in the rastergrams, averaged 37 ms in length (range: 14–70 ms) across all files analyzed. Spike counts within this time window were then plotted as a function of tone intensity and frequency, and the outline of the frequency-intensity tuning curve was estimated by eye. Although responses to both low- and high-frequency stimulus sets were collected at each recording site, the stimulus-evoked response and frequency-intensity tuning curve usually fell mostly within one frequency range or the other, and so further analyses for each site were performed only on the recording in the appropriate stimulus range.

Response characteristics were subsequently defined with reference to this frequency-intensity tuning curve. The *threshold* was chosen to be the minimum stimulus intensity included in the frequency-intensity curve, and the *characteristic frequency (CF*) was the tone frequency that evoked a response at threshold. *Bandwidth* at 10 dB above threshold was the frequency width of the tuning curve at that intensity level; *normalized BW10* was then defined to be this bandwidth normalized by the CF (i.e., the inverse of Q10). The *first-spike latency* was chosen to be the apparent asymptote in a plot of response latency versus increasing stimulus intensity for tone burst frequencies within 1/10 octave of the CF. Finally, the *response duration* was defined as the time from the start of the response (defined by the first-spike latency) to the end of the peak in the PSTH formed by averaging responses to the subset of stimuli that fell within the frequency-intensity range of the tuning curve. More precisely, the end of this PSTH peak was usually defined as the time at which the spike rate fell to within 1 SD of the mean spontaneous firing rate; this time value was occasionally corrected if it did not correspond well to the apparent end of the response peak that would have been chosen by eye. This method for determining response duration thus produced a measure that represented the time from the beginning of the earliest response to the end of the longest response within the frequency-intensity tuning curve. To address the possibility that this measure of response duration could be biased by large variations in response latency or duration for different stimuli within the frequency-intensity tuning curve, the data were also analyzed using a much more restricted, threshold-dependent measure of response duration. This alternative measure of response duration was based on a PSTH constructed only from responses to stimuli with frequencies within 1/10 octave of the CF and amplitudes within 10 dB of threshold, and was defined as the width of the first peak in the restricted PSTH that exceeded the mean spontaneous firing rate by 1 SD.

Dynamic random chord stimuli

The dynamic random chord stimuli used in these experiments were similar to those used in previous studies (deCharms et al. 1998; Rutkowski et al. 2002; Schnupp et al. 2001) except that the intensity of component tone pulses was variable. A schematic spectrographic representation of the stimulus is shown in Fig. 2*A*. Tone pulses were 20 ms in length, ramped up and down with 5-ms cosine gates. The times, frequencies, and sound intensities of all tone pulses were chosen randomly and independently within the discretizations of those variables (20-ms bins in time, 1/12-octave bins covering either 2–32 or 25–100 kHz in frequency and 5-dB-SPL bins covering 25–70 dB SPL in sound level). At any time point, the stimulus averaged two tone pulses per octave, with an expected loudness of 73 dB SPL for the low-frequency stimulus and 70 dB SPL for the high-frequency stimulus. Each stimulus trial was 60 s in duration and was repeated either 20 times (for the low-frequency stimulus) or 10 times (for the high-frequency stimulus) at each site. Sound presentation from one trial to the next was continuous with no inter-trial interval; thus the total duration of playback was 20 min for the low-frequency stimulus and 10 min for the high-frequency stimulus.

Analysis of responses to dynamic random chord stimuli

STRF ESTIMATION. Responses to dynamic random chord stimuli that exhibited extreme instability in total spike count over the 10- or 20-min stimulus presentation time were discarded from the data set before STRF estimation. Because minor instability in a long recording cannot easily be distinguished from true neuronal response variability, we chose as conservative a threshold as possible for rejection of recordings. The criterion for rejecting a recording was that the Fano factor (variance divided by mean) for the total number of spikes per 60-s trial had to exceed 200; that is, the trial-to-trial spike-count variance had to be $>$200 times greater than would be expected from a Poisson process. We considered this criterion to be an appropriately conservative threshold for data rejection because Fano factors typically reported for cortex are at least an order of magnitude smaller than this threshold (Kisley and Gerstein 1999; Tolhurst et al. 1983) and because the few recordings with Fano factors $>$200 tended to exhibit smooth variations in firing rate over the 10- to 20-min recording time that seemed very likely to be related to changes in the animal's anesthetic state. Only 7 of 198 STRF recordings (3.5%) were rejected for exceeding the Fano factor threshold of 200, and the majority of the remaining recordings had Fano factors $<$10.

Histograms of the neuronal responses to dynamic random chord stimuli were constructed by collecting spikes from all 10–20 trials of the sorted spike trains (e.g., Fig. 2*B*) into 20-ms bins aligned with the tone-pulse components of the stimuli (e.g., Fig. 2*C*). STRFs for each recording site were then estimated as explained in the following text, using the histogrammed responses and a spectrographic representation of the stimulus in terms of tone-pulse times, frequencies, and amplitudes. Thus both stimulus and response were treated as discrete-time

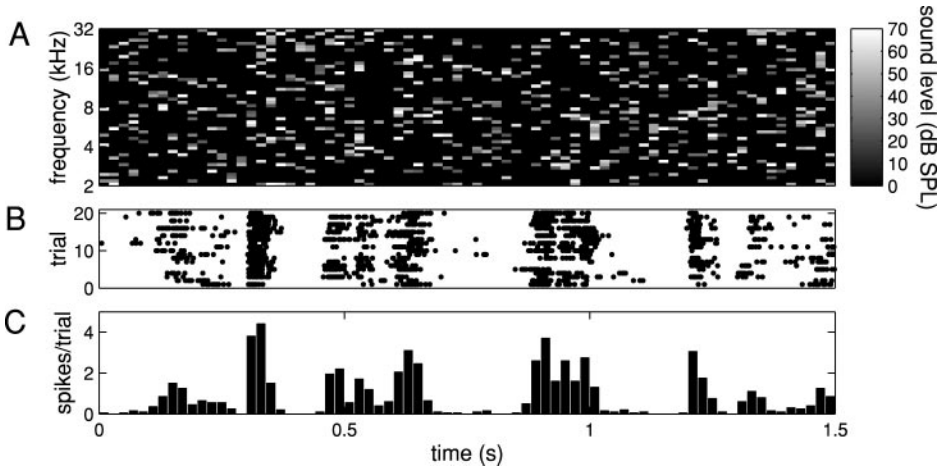

FIG. 2. Dynamic random chord stimulus and corresponding stimulus-evoked responses from a mouse auditory cortex recording. *A*: spectrographic representation of a 1.5-s segment of the low-frequency dynamic random chord stimulus. Each shaded rectangle represents a 20-ms cosine-gated tone pulse centered on the indicated frequency and time, with a maximal intensity given by the depth of shading. The high-frequency dynamic random chord stimulus was similar in structure but covered 25–100 kHz in frequency rather than 2–32 kHz. *B*: measured neuronal response to the segment of the dynamic random chord stimulus shown in *A* displayed as trial-by-trial spike rasters. *C*: histogram of spikes per trial in 20-ms bins aligned with the tone pulses in the stimulus. Time is shown relative to the beginning of the stimulus excerpt, which was taken from the middle of a 60-s stimulus trial. The spectrotemporal receptive field (STRF) estimation procedure involved regression of the histogrammed neuronal response against the stimulus, a process mathematically similar to reverse correlation on the histogram.

processes, with the time step (20 ms) given by the duration of tone-pulse components of the dynamic random chord stimuli. The strong autocorrelations present in the stimuli at all shorter time scales made STRFs estimated with finer temporal precision noisier than STRFs estimated with this 20-ms time step. Our Bayesian estimation techniques (see following text) were designed to reduce noise in STRF models by eliminating noisier modes of the models and smoothing the reliable modes; since the reliable modes were those at a 20-ms time scale, it was not productive to estimate the STRF with a finer temporal precision than 20 ms.

Conceptually, the STRF estimation procedure used here was similar to reverse-correlation on the response histogram or, more precisely, to computation of an optimally smoothed and de-noised, autocorrelation-corrected, spike-count-weighted average of 300-ms stimulus segments preceding each 20-ms bin in the histogram. Mathematical details of our STRF estimation method, called automatic smoothness determination and relevance determination (ASD/RD), are given elsewhere (Sahani and Linden 2003a) and are described only briefly here. Bayesian techniques were first used to derive optimal spectral and temporal smoothing and scale parameters for each recording. The STRF was then estimated by *maximum a posteriori* linear regression between the response histogram and stimulus, using the previously determined optimal smoothing and scale parameters to set the prior distribution on the weights. Linear regression with no smoothing or scaling prior yields exactly the same result as the discrete-time Wiener filter usually associated with reverse correlation (Aertsen and Johannesma 1981). When combined with Bayesian smoothing and scale selection as done here, regression yields STRF estimates that are better able to predict neuronal responses to novel data than the conventional Wiener filter (Sahani and Linden 2003a). Thus this procedure provides a better estimate of the true spectrogram-linear component of the neuronal response function than does the Wiener filter, which overfits more severely to the noise inevitably present in the limited available data. Other researchers have previously used different methods (for example, elimination of singular-value decomposition components of the Wiener filter by cross-validation) (Theunissen et al. 2001) to pursue the same goal of obtaining improved STRF estimates.

Predicted neuronal responses were computed from each STRF by convolving the STRF with a time-frequency representation of the stimulus. Specifically, the predicted firing rate for each 20-ms time bin of the response histogram was the dot-product between the 300-ms-long STRF and the time-frequency representation of tone amplitudes in the 300-ms stimulus segment preceding that time bin. The prediction error for the STRF was then determined by comparing predicted and measured responses to novel segments of the dynamic random chord stimulus (i.e., stimulus segments that were not used for STRF estimation). The average prediction error was estimated by cross-validation, a standard statistical procedure (Duda and Hart 1973) performed as follows. Each stimulus trial was divided 10 times into a training segment and a test segment (9/10 and 1/10 of the 60-s stimulus trial length, respectively), such that the 10 test segments were all disjoint. Ten STRF estimates were then obtained from the histogrammed neuronal responses to each of the 10 different training segments. For each of these 10 STRFs, we calculated the mean squared error between the histogrammed response to the test segment that would be predicted based on the STRF and the corresponding histogram of actual measured responses to the test segment. These mean squared errors for each of the ten data subdivisions were then averaged together to yield the final estimated prediction error. A standard error on the estimated prediction error was also obtained, by dividing the SD of the mean squared error estimates for the 10 data subdivisions by the square root of the number of data subdivisions. Recordings for which the STRF prediction error was $\geq$2 SEs smaller than could be achieved by simply predicting a constant mean response were deemed *predictive STRFs*. Only these predictive STRFs (114 of 191 STRFs; see RESULTS) were included in the final analysis of STRF characteristics.

There are two reasons why some recordings might have failed to yield predictive STRFs. The responses of the neurons might have been largely nonlinear in the spectrogram of the stimulus and therefore not predictable from the spectrogram-linear STRFs. Alternatively (or additionally), the signal-to-noise levels in those recordings might have been too low for the predictive capabilities of the STRFs to be detected. In work described elsewhere (Sahani and Linden 2003b), we have shown that rodent auditory cortex responses to dynamic random chord stimuli, including the mouse auditory cortex responses considered in the present paper, are significantly nonlinear. Consistent with this observation, we found that factors associated with low signal-to-noise levels, such as low spike count and high trial-to-trial variability,

could account only in part for failures of recordings to yield predictive STRFs.

STRF CHARACTERIZATION. Analysis of various features of STRFs, including temporal and spectral profiles and spectrotemporal inseparability (see following text), was based on mathematical decomposition of the STRF matrix. The STRF can be viewed as a matrix of weights R in time-frequency space with each row corresponding to a single frequency and each column to a single time lag (Fig. 3*A*). These weights correspond mathematically to the regression coefficients from the STRF estimation and conceptually to the sensitivity of the neuron to different frequencies at different times preceding a spike. Like any other matrix, the STRF matrix can be decomposed into a series of uncorrelated components, each consisting of a single vector along one dimension (time) and a single vector along the other (frequency). These components can be recombined completely to obtain the original matrix or recombined in subsets to yield various approximations to the original matrix. The process of finding these components for rectangular matrices (such as the 15 time bin by 24 or 48 frequency bin STRFs considered here) is called singular value decomposition (SVD).

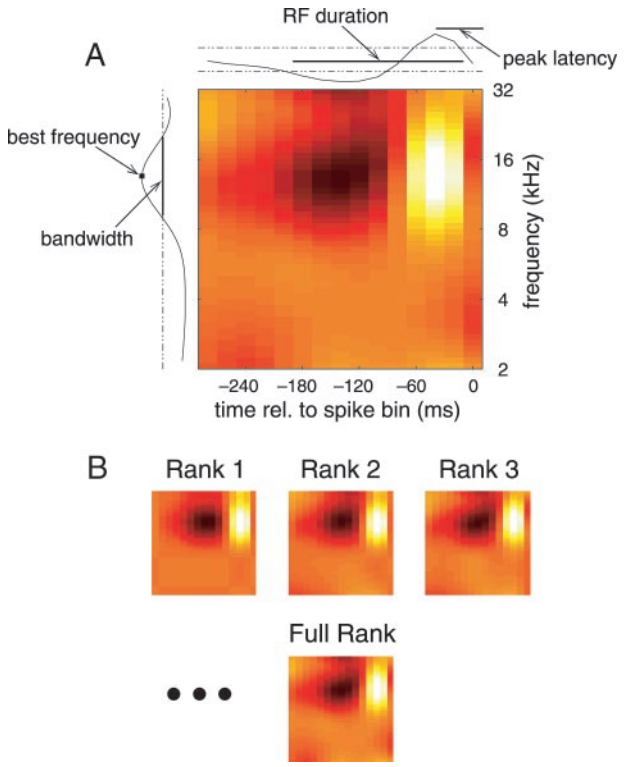

FIG. 3. Analysis of STRFs. *A*: temporal and spectral profile measures. Time is shown relative to the time bin for which the firing rate is to be predicted. Color scale in the STRF indicates regression weight, increasing from black (large negative weight) through dark red to medium orange (zero weight) to yellow to white (large positive weight). Regression weight can be equated with stimulus sensitivity; thus this example STRF suggests that the neuron will be most active ~40 ms after the onset of a 14-kHz tone pulse. The temporal and spectral profiles of the STRF, obtained from singular value decomposition of the STRF matrix, are shown along the top and left sides of the STRF. *B*: evaluation of spectrotemporal separability. Approximations to the full STRF can be constructed by recombining components of the STRF matrix singular value decomposition in order of decreasing singular value. This procedure was used to obtain, for each STRF, a separable (rank 1) model along with an inseparable model of rank 3, which optimized the trade-off between minimizing the number of model parameters and capturing structure evident in most of the full STRFs. If the rank 3 inseparable model of a STRF predicted neuronal responses to novel stimulus segments significantly more accurately than the separable model did, the STRF was judged to be inseparable. See METHODS for details.

The SVD of the time-frequency STRF matrix was calculated as $R = USV$, with the rows and columns of the factor matrices U, S, and V arranged so that the singular values along the diagonal of S appeared in decreasing order. In this representation, the product of the first column of U with the first row of V, scaled by the first singular value, gives the spectrotemporally separable matrix (or *separable model*) that best approximates the full STRF matrix R in the least-squares sense. Thus the first column of U and first row of V may be taken to represent the spectral profile and temporal profile for the full STRF (illustrated in Fig. 3*A* as curves along the left and top edges of the STRF). Like the comparable approach used in Depireux et al. (2001), this procedure is preferable to averaging across time or frequency to obtain spectral or temporal profiles, because such averages would be confounded by reversals in tuning polarity along the averaged dimension (such as the alternation of dark and light regions along the time dimension in Fig. 3*A*); it is also preferable to analyzing time or frequency slices through the peak in the STRF, because peak-dependent definitions of spectral or temporal profiles would be more sensitive to noise in the STRF estimation procedure.

Temporal and spectral properties of the receptive fields were defined based on the temporal and spectral profiles as illustrated in Fig. 3*A*. The *peak latency* was the time to the center of the peak in the first subfield of the receptive field (usually an excitatory subfield, but occasionally an inhibitory subfield). *Excitatory subfield duration* was defined to be the width at half-maximum of the positive peak in temporal profile, and *inhibitory subfield duration* was defined to be the width at half-minimum of the negative peak in the temporal profile. The *receptive-field duration* was then defined as the time from the beginning of the first subfield to the end of the last subfield, a measure insensitive to the ordering of excitatory and inhibitory subfields. In the spectral profile, the *best frequency* was the frequency corresponding to the absolute maximum (larger of positive or negative peaks) in the spectral profile. The *bandwidth* was then defined to be the width at half-height of that spectral peak, and the *normalized bandwidth* was this bandwidth normalized by the best frequency.

STRF INSEPARABILITY. Time-frequency inseparability of the STRF was assessed by comparing the predictive capabilities of rank 1 (separable) and rank 3 (inseparable) SVD approximations to the full STRF matrix. As noted in the preceding text, the best separable (i.e., rank 1) approximation to the full STRF R is the matrix formed by the product of the first column of U, first element of S, and first row of V. More generally, the matrix formed from the product of the first n columns of U, first $n \times n$ block of S and first n rows of V gives the best rank n approximation to R in the least-squares sense (Fig. 3*B*). Higher values of n will produce increasingly accurate approximations to R; however, higher-rank models often performed poorly at predicting responses to novel stimulus segments, indicating greater overfitting to noise. We chose a rank of 3 to optimize the trade-off between minimizing the model rank and capturing potentially important inseparable structure in the full STRFs, on the basis of two observations. First, when we used a Bayesian de-noising technique related to our STRF estimation method (Sahani and Linden 2003a) to choose the number of relevant SVD components for each STRF, we found that the distribution of resulting ranks had a mode of 3. Second, we noticed that STRF approximations of rank 3 were usually qualitatively indistinguishable from full-rank STRFs; that is, the rank 3 approximations generally captured what appeared by eye to be structure rather than noise in the full STRFs.

Predictive capabilities of the separable and rank 3 inseparable models for each STRF were determined by a cross-validation procedure like that described in the previous section on STRF estimation. We divided the data into a training segment and a test segment (9/10 and 1/10 of each stimulus trial, respectively), estimated a full STRF from the training segment, and computed the SVD of this STRF to obtain its separable and rank 3 inseparable approximations. Then we predicted neuronal responses in the test segment of the data using both

the separable and rank 3 inseparable models, calculated the error in these predictions as described previously, and computed the difference in error between the two predictions. Repeating this procedure for each of 10 disjoint divisions of the data into a training segment and a test segment, we were able to obtain both an estimate of the average difference in prediction error between the two models, and a SE on this estimate. If the average difference in prediction error between the separable model and rank 3 inseparable model was ≥2 SEs greater than zero, then the STRF was declared to be significantly inseparable. In other words, an inseparable STRF was one for which the rank 3 inseparable model predicted responses to test data significantly more accurately than did the separable model. Because the null hypothesis was that the STRF was separable, this approach gave us a conservative test for inseparability. STRFs that were judged to be not significantly inseparable might either be truly separable or else simply not distinguishable from separable given our limited data.

To obtain the prediction-based inseparability index used in population data plots, the average difference in prediction error between the separable model and rank 3 inseparable model was normalized by an estimate of the total predictable stimulus-related power in the neuronal response [the "signal power"; see Sahani and Linden (2003b) for details on the derivation of this quantity]. Thus a value of 0.1 for the prediction-based inseparability index would mean that the inseparable model predicted 10% more of the stimulus-related power in the neuronal response than the separable model. [We have shown elsewhere (Sahani and Linden 2003b) that rodent auditory cortical responses to dynamic random chord stimuli are so nonlinear that linear STRF models typically capture no more than half of the stimulus-related response power; therefore a change of 10% could represent a substantial improvement in response prediction.] For comparison with previous studies, we also quantified inseparability with a SVD-based inseparability index previously used for characterizing STRFs from ferret auditory cortex (Depireux et al. 2001) and related to similar measures used in other studies (e.g., Sen et al. 2001). This index, called α_{SVD} in Depireux et al. (2001), quantifies the concentration of power in higher singular values of the STRF matrix SVD

$$\alpha_{SVD} = 1 - \frac{S_1^2}{\sum_{i=1}^{N} S_i^2},$$

where S is the vector of singular values arranged in order of decreasing amplitude. We applied this inseparability measure both to the full STRF, for comparison with our prediction-based inseparability index, and also to the first and second quadrants of the two-dimensional Fourier transform of the STRF, to evaluate the "quadrant separability" of our STRFs as defined by Depireux et al. (2001).

Population analyses

Population distributions were compared using the two-sample Kolmogorov-Smirnov test, a nonparametric test of the null hypothesis that two distributions are similar (Lindgren 1993). Correlations between measured population variables were quantified with the nonparametric Spearman rank correlation test; population fractions were compared with Fisher's exact test; and differences in population means were assessed with the two-sample Student's *t*-test (Lindgren 1993; Zar 1996). The *t*-test results on means are reported in preference to nonparametric Wilcoxon rank-sum test results on medians because the two-sample *t*-test is more robust than the Wilcoxon rank-sum test to violations of the assumption that the two distributions under consideration have the same shape, and because the Gaussian approximation to the posterior mean distribution inherent in the *t*-test was not unreasonable given the sample sizes. However, in all cases in which a significant difference in population means is reported, the difference in population medians was also significant according to the Wilcoxon rank-sum test.

Results of all statistical tests were deemed significant if the null hypothesis was rejected at a significance level of 0.05. Throughout the text, "K-S test" is used as an abbreviation for "two-sample Kolmogorov-Smirnov test," and "*t*-test" implies "two-sample Student's *t*-test." Test statistic values are reported as D_n for the K-S test and t_n for the *t*-test, where n is the number of degrees of freedom, r_s is the Spearman rank correlation coefficient. All tests are identified as 1- or 2-tailed in the text as appropriate for the alternative hypothesis being tested.

RESULTS

Database characteristics

Neuronal responses to prolonged dynamic random chord stimuli and simple tone bursts were recorded at 35 AI sites and 31 AAF sites. Multiunit responses to tone bursts, used to determine the position of each recording site in the AI–AAF tonotopy, revealed no significant differences between the distributions of characteristic frequencies or response thresholds for AI and AAF recording sites (2-tailed K-S tests and *t*-tests). As shown in Fig. 4, the CF values for AI sites ranged from 6 to 40 kHz and thresholds varied from 4 to 36 dB SPL; for AAF sites, CFs were 10–35 kHz and thresholds 4–39 dB SPL.

Off-line spike sorting and analysis of electrode signals continuously recorded during presentation of low- and high-frequency dynamic random chord stimuli at each site yielded a total of 191 STRFs. There were no significant differences observed between AI and AAF responses to dynamic random chord stimuli in either noise level [see Sahani and Linden (2003b) for details on the noise power calculation] or stability of firing rate across repeated trials (quantified as the inverse Fano factor). Moreover, applying analysis techniques described at length in Sahani and Linden (2003b), we found no significant differences in the goodness-of-fit of linear STRFs for AI versus AAF, nor for low- versus high-frequency recordings. Of the 191 STRF recordings analyzed, 114 (60 from AI and 54 from AAF) proved to be predictive; that is, these STRFs could be used to obtain significantly more accurate predictions of neuronal responses to novel stimulus segments than could be achieved based on knowledge of the mean firing rate alone (see METHODS). These 114 predictive STRFs form the database for all further STRF analyses presented in RESULTS.

Because responses to low- and high-frequency dynamic

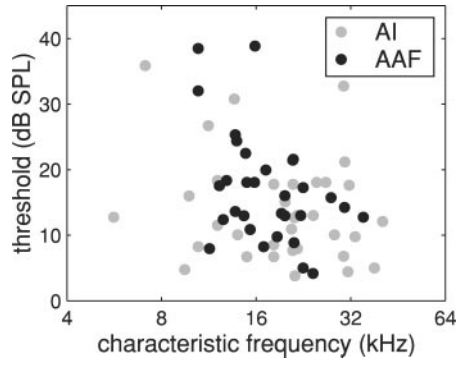

FIG. 4. Recording site characteristics. Multiunit responses to isolated tone bursts varying in frequency and intensity were analyzed to extract the response threshold and characteristic frequency for each recording site. The distributions of threshold versus characteristic frequency for recording sites in AI (◎) and AAF (●) were overlapping, with no significant differences between the 2 populations along either dimension.

random chord stimuli were recorded and analyzed separately at each site and because an average of 1.5 distinct single units or small neuronal clusters could be extracted from each recording by spike-sorting, many recording sites produced multiple predictive STRFs. STRFs in the same frequency range recorded at the same site could be assumed to have arisen from different neurons or distinct neuronal clusters because the spike waveforms had been discriminated during spike sorting. However, because responses to low- and high-frequency dynamic random chord stimuli were recorded and analyzed separately, low- and high-frequency STRFs obtained from the same recording site might have arisen either from distinct neurons or neuronal clusters or from the same neuron or neuronal cluster responding to both low- and high-frequency stimuli. Definitive identification of the same spike waveform in separate low- and high-frequency recordings was often not possible; therefore, we pooled data from all predictive STRFs in the analyses shown here, regardless of stimulus frequency range or site of recording. To address the possibility that our results could have been affected by the inclusion in the database of separate high- and low-frequency STRFs for the same neurons, we also re-analyzed all the data using only low-frequency STRFs, which formed the majority (71%) of the predictive STRFs. All results obtained using a database restricted to low-frequency STRFs were similar to those reported in the following text for the database pooling high- and low-frequency STRFs.

Data from single-unit and cluster recordings were also pooled in all STRF analyses. Among the recordings in the STRF database, 40% from AI and 15% from AAF appeared to be single units based on the combined results of Bayesian spike-sorting (Lewicki 1994) and visual inspection of spike waveforms chosen randomly from throughout each 10- or 20-min recording. No significant differences between STRFs derived from single-unit recordings and STRFs obtained from cluster recordings were observed for any of the receptive-field parameters examined here. Figure 5 displays six representative mouse STRFs from AI and AAF and illustrates the similarity of single-unit and cluster STRFs; there are no clear differences

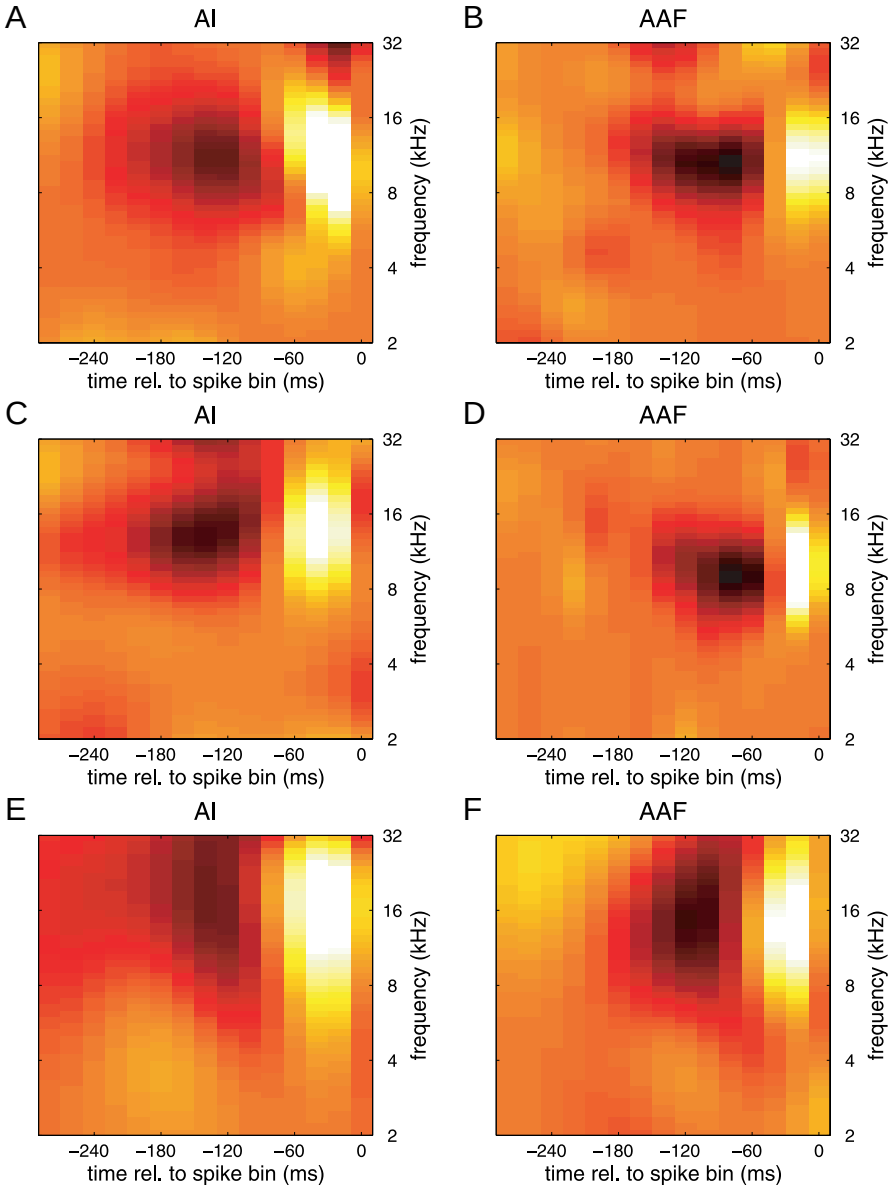

FIG. 5. Examples of STRFs from mouse auditory cortex. As in Fig. 3, light and dark areas in each plot correspond, respectively, to excitatory and inhibitory subregions of the receptive field, and orange background indicates no stimulus sensitivity (i.e., regions outside the receptive field). Color shading was scaled independently for each plot to fit the range of spectrotemporal weights in each STRF, with medium orange fixed to regression weight 0. Negative time axis indicates time preceding the time bin in which spikes evoked by the stimulus would occur. Each STRF may therefore be viewed as a spectrogram-linear estimate of the preferred stimulus for the neuron, which would be a sound onset with slightly different frequency content and AM characteristics for each example shown. *A*, *C*, and *E*: AI STRFs. *B*, *D*, and *F*: AAF STRFs. The STRFs in *B* and *E* were derived from single-unit recordings, whereas the other STRFs were obtained from cluster recordings. Note that the single-unit and cluster STRFs appear to be very similar in structure and that the time course of the AI STRFs is generally more elongated than that of the AAF STRFs.

between the STRFs derived from single-unit recordings in Fig. 5, *B* and *E*, and the cluster STRFs shown in the other panels of the figure.

STRF temporal structure

The examples of AI and AAF STRFs shown in Fig. 5 demonstrate the observed temporal differences between AI and AAF. All six STRFs in the figure suggest tuning to sound onsets in a similar frequency range, but the temporal structure of the AI STRFs (Fig. 5, *A*, *C*, and *E*) differs from that of the AAF STRFs (Fig. 5, *B*, *D*, and *F*) in two ways. First, the peaks of the excitatory subfields (lightest regions) are shifted farther left in the AI than in the AAF STRFs. This shift indicates that there was a longer delay for the AI neurons than for the AAF neurons between the moment at which a preferred stimulus occurred, and the time at which the neuron most reliably fired a spike; in other words, the STRF peak latency was longer for these AI neurons than for the AAF neurons. Second, the combined excitatory and inhibitory subfields (light and dark regions, respectively) seem to extend across more time bins in the AI than in the AAF STRFs. This elongation implies that the preferred stimuli (or more precisely, the stimuli that would best activate the linear filter approximation to the true neuronal response function) for the AI neurons were more slowly modulated in amplitude than the preferred stimuli for the AAF neurons, or equivalently, that excitatory/inhibitory receptive-field duration was longer for the AI than the AAF example neurons.

These observations hold across the database of AI and AAF STRFs, as shown in Fig. 6. Distributions of STRF peak latencies were different for AI and AAF (Fig. 6*A*); the AI distribution was significantly shifted to larger values (1-tailed K-S test, $P < 0.0005$, $D_{114} = 0.39$), and the mean peak latency was 17 ms longer for AI than for AAF (mean ± SE, 44 ± 2 ms for AI and 27 ± 2 ms for AAF; 1-tailed *t*-test, $P < 0.0001$, $t_{112} = 5.87$). Similarly, despite their considerable overlap, the distributions of AI and AAF receptive-field durations differed (Fig. 6*B*), again with a significant shift in the AI distribution toward larger values (1-tailed K-S test, $P < 0.0001$, $D_{114} = 0.39$). Mean receptive-field duration was nearly 30 ms longer for AI than for AAF (135 ± 5 ms for AI and 108 ± 4 ms for AAF; 1-tailed *t*-test, $P < 0.0001$, $t_{112} = 3.94$). Excitatory subfields appeared to contribute more to this difference in receptive-field duration than inhibitory subfields, but both excitatory and inhibitory subfield durations were significantly longer in AI than in AAF (1-tailed K-S tests and *t*-tests, $P < 0.05$ in all cases; subfield data not shown). Thus both peak latency and receptive-field duration were longer for STRFs in AI than in AAF, and the difference in receptive-field duration involved both excitatory and inhibitory subfields.

As would be expected given these differences between AI and AAF, peak latency and receptive-field duration were significantly correlated across the entire STRF database; the correlation was strongest for peak latency and excitatory subfield duration (2-tailed Spearman rank correlation test, $r_s = 0.65$, $P < 0.0001$). Peak latency and excitatory subfield duration were also correlated within AI alone ($r_s = 0.72$, $P < 0.0001$), and (less strongly) within AAF alone ($r_s = 0.29$, $P < 0.05$), indicating that these temporal properties of receptive fields co-varied not only between auditory fields but also across STRFs recorded within each field.

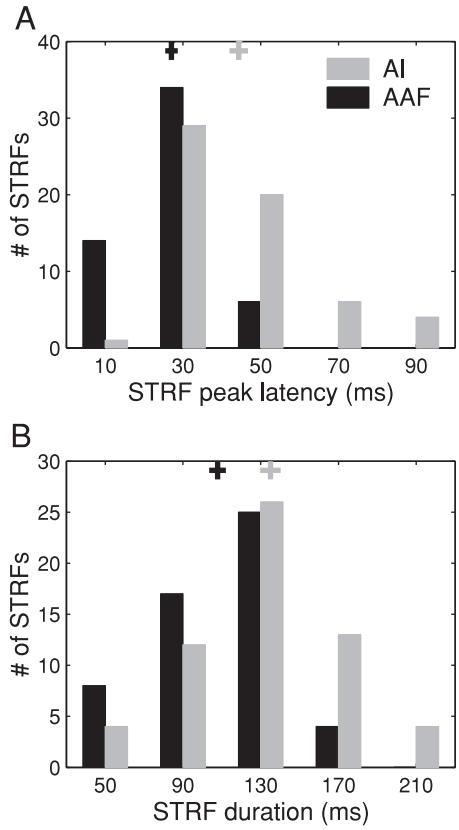

FIG. 6. Temporal differences between AI and AAF STRFs. +, the mean for each population with the total width of the horizontal line in each symbol indicating 2 SEs. ▨, AI data; ■, AAF data. *A*: STRF peak latencies. *B*: receptive-field durations, encompassing excitatory and inhibitory subfields. Both peak latencies and receptive-field durations were significantly longer in AI than in AAF.

STRF spectral structure

As suggested by the examples shown in Fig. 5, AI and AAF STRFs appeared to be more similar in spectral structure than in temporal structure; however, some small differences between the two auditory fields were evident in the population analyses. STRFs in both areas had broad frequency tuning, but the STRF bandwidths tended to be slightly larger in AI than in AAF. Figure 7 displays the distributions of normalized bandwidth (STRF peak width at half-height, normalized by STRF best frequency) for all STRFs in which the STRF peak did not fall near the edge of the STRF frequency range (61 of the 114 predictive STRFs). The normalized bandwidth distribution for AI was significantly shifted to larger bandwidths (1-tailed K-S test, $P < 0.005$, $D_{61} = 0.43$), and the mean bandwidth for AI was larger than for AAF (mean ± SE, 1.14 ± 0.10 for AI and 0.86 ± 0.08 for AAF; 1-tailed *t*-test, $P < 0.05$, $t_{59} = 2.21$). Thus while frequency tuning was broad in both auditory areas, STRF bandwidths were broader in AI than in AAF. Because AI STRFs also tended to have longer times to peak and longer receptive-field durations than AAF STRFs, spectral and temporal STRF measures were correlated across the entire population of recorded STRFs (2-tailed Spearman rank correlation test, $P < 0.05$ for all comparisons). This trend toward co-

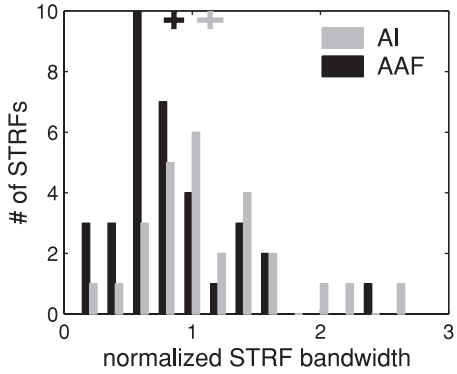

FIG. 7. Spectral differences between AI and AAF STRFs. Normalized bandwidth is defined as frequency width at half-height of the STRF peak, normalized by the peak frequency (see METHODS). STRFs for which the peak fell at an edge of the frequency range were excluded from this analysis because no reliable estimate of STRF bandwidth could be obtained in those cases. Other conventions as in Fig. 6. Note that although STRFs in both AI and AAF had broad frequency tuning, the STRF bandwidths in AI tended to be slightly larger than those in AAF.

variation in spectral and temporal measures was also evident within AI alone but did not reach significance within AAF alone.

In addition to their rather broad bandwidths, recordings from AI and AAF often shared another spectral characteristic: ultrasound sensitivity. While most of the recording sites produced only low-frequency STRFs, more than one-third of the 66 recording sites (13 sites in AI, 13 sites in AAF) yielded predictive STRFs in both the low (2–32 kHz)-and high (25–100 kHz)-frequency ranges. (Frequency-intensity tuning curves collected at these sites also showed both low-frequency and ultrasound sensitivity.) Of these 26 sites, 11 sites (3 in AI, 8 in AAF) gave low- and high-frequency STRFs with clearly distinct low- and high-frequency peaks; 13 sites (9 in AI, 4 in AAF) yielded STRFs that displayed broad frequency tuning extending smoothly from low frequencies to 50 kHz or above; and the remaining 2 sites (1 each in AI and AAF) produced ultrasound STRFs with high-frequency sensitivity confined to the 25- to 32-kHz region of overlap between the two stimulus frequency ranges.

Figure 8 shows ultrasound STRFs of the first type, derived from sites that were judged during mapping with tonal stimuli to be tuned to lower frequencies consistent with the tonotopic organization of AI and AAF. All four of these recording sites also produced predictive low-frequency STRFs with distinct receptive-field peaks below 25 kHz, as well as frequency-intensity tuning curves with low-frequency tuning peaks but also some sensitivity in the ultrasound range (not shown). Our single-electrode recordings did not provide definitive proof that the same neurons were responding both to lower frequencies and to higher frequencies at these sites; indeed, it is possible that the low- and high-frequency responses at these sites reflect the sensitivities of separate and differently tuned neurons. However, in either case, the results indicate that neurons with ultrasound sensitivity exist at recording sites judged to be within the boundaries of AI and AAF as well as within the previously defined ultrasound field.

STRF spectrotemporal structure

Analysis of temporal or spectral properties of STRFs requires the simplifying assumption that STRFs may be viewed as separable so that the temporal or spectral profiles of the receptive field can be examined separately. This simplification, although useful for highlighting obvious differences between AI and AAF, obscures the complexity that was observed in some of the mouse STRFs. Nearly one-quarter of the STRFs recorded in both AI and AAF had significantly inseparable spectrotemporal structure—i.e., structure that could not be described fully without reference to an interaction between spectral and temporal features of the receptive field. Three representative examples of such spectrotemporally inseparable STRFs are shown in Fig. 9. Each set of two panels displays the separable model of the STRF on the left, for comparison with the rank 3 inseparable model of the STRF (see METHODS) on the right. (For most STRFs, including these 3 examples, the rank 3 inseparable model was nearly indistinguishable by eye from the full STRF.) As explained in METHODS, these STRFs were judged to be inseparable because the inseparable model significantly outperformed the separable model at prediction of neuronal responses to novel segments of the dynamic random chord stimulus. Inseparable features of the STRFs, which presumably account for the improvements in response prediction, can be identified by comparing the two models. In Fig. 9*A*, the inseparability appears as offset excitatory and inhibitory subfields in the inseparable model; the excitatory subfield is

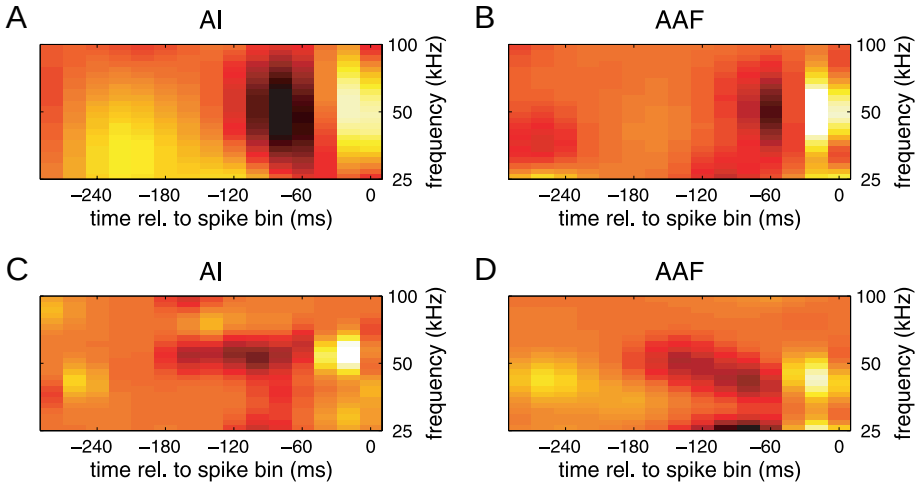

FIG. 8. Examples of ultrasound STRFs. All recordings were made at sites judged to be in AI (*A* and *C*) or AAF (*B* and *D*) on the basis of tonotopic mapping with low- and high-frequency tone bursts, and all 4 sites produced predictive low-frequency STRFs with distinct receptive-field peaks below 25 kHz. The AI ultrasound STRF in *C* was derived from a single-unit recording; the other STRFs shown were obtained from cluster recordings. Other plotting conventions are as in Fig. 5.

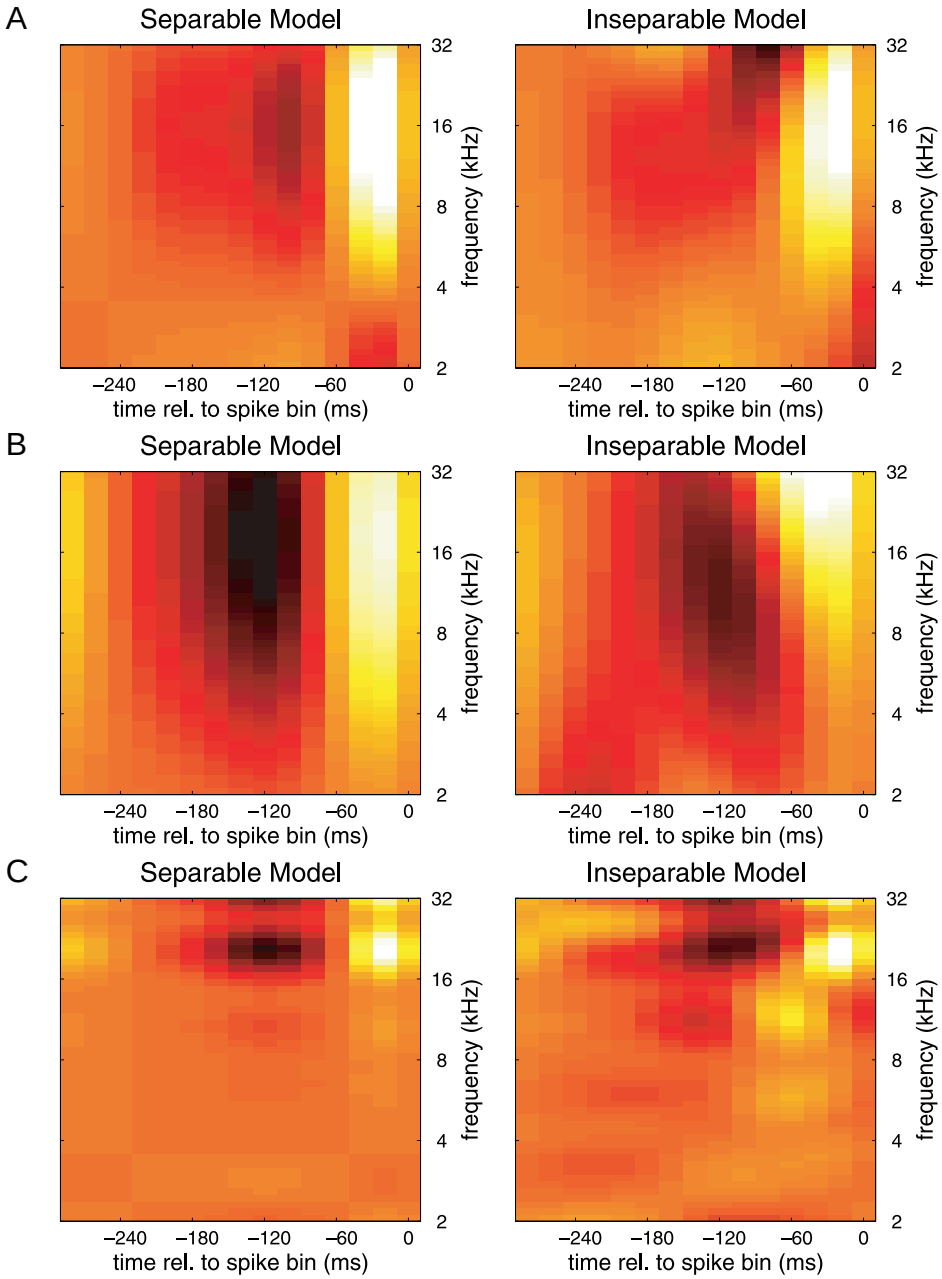

FIG. 9. Examples of inseparable STRFs. Each row of panels displays the separable model (*left*) and rank 3 inseparable model (*right*) for the same STRF. For all 3 examples shown, the inseparable model predicted neuronal responses to novel stimulus segments significantly more accurately than the separable model did. *A*: AI STRF from a single-unit recording. The excitatory and inhibitory subfields are offset both spectrally and temporally in the inseparable model; this spectrotemporal feature is not captured in the separable model. *B*: AAF STRF from a cluster recording. Note the pronounced slant in the inseparable model of the receptive field. *C*: AAF STRF, from a cluster recording. The inseparable model in this case has multiple offset excitatory and inhibitory subfields and also a spectrotemporal slant in the receptive field.

shifted to lower frequencies than the inhibitory subfield preceding it. The inseparable model in Fig. 9*B* displays a different form of inseparability: a smooth slant in both the excitatory and inhibitory portions of the receptive field, suggesting tuning to fast frequency sweeps. Figure 9*C* combines features of both of the other two examples in what appear to be multiple stacked excitatory and inhibitory subfields displaced along a spectrotemporal slant.

Across the population, a total of 26/114 STRFs (23%) had significantly inseparable spectrotemporal structure, like that shown in the examples in the preceding text. Significantly inseparable STRFs appeared in similar proportions in both areas AI and AAF (16/60 STRFs in AI versus 10/54 STRFs in AAF; Fisher's exact text, $P > 0.5$), and among both single-unit and cluster recordings (8/32 single-unit STRFs vs. 18/82 cluster STRFs; Fisher's exact test, $P > 0.8$). There were no significant differences between AI and AAF STRFs (or single-unit or cluster STRFs) in their degree of spectrotemporal inseparability, so all data from the two auditory fields were pooled in Fig. 10*A* to illustrate the total population spread in two measures of STRF inseparability. The prediction-based inseparability index, explained in METHODS, quantifies the improvement in neuronal response predictions that could be obtained using an inseparable rather than a separable STRF model. Significantly inseparable STRFs (i.e., those for which the prediction-based inseparability index was significantly greater than 0) are indicated (●) in the scatter plot and in both marginal histograms. The distribution of the prediction-based inseparability index is compared in the scatterplot to the distribution of a SVD-based inseparability index similar to that used in previous studies of STRF inseparability (Depireux et al. 2001; cf. Sen et al. 2001). Values of the two inseparability

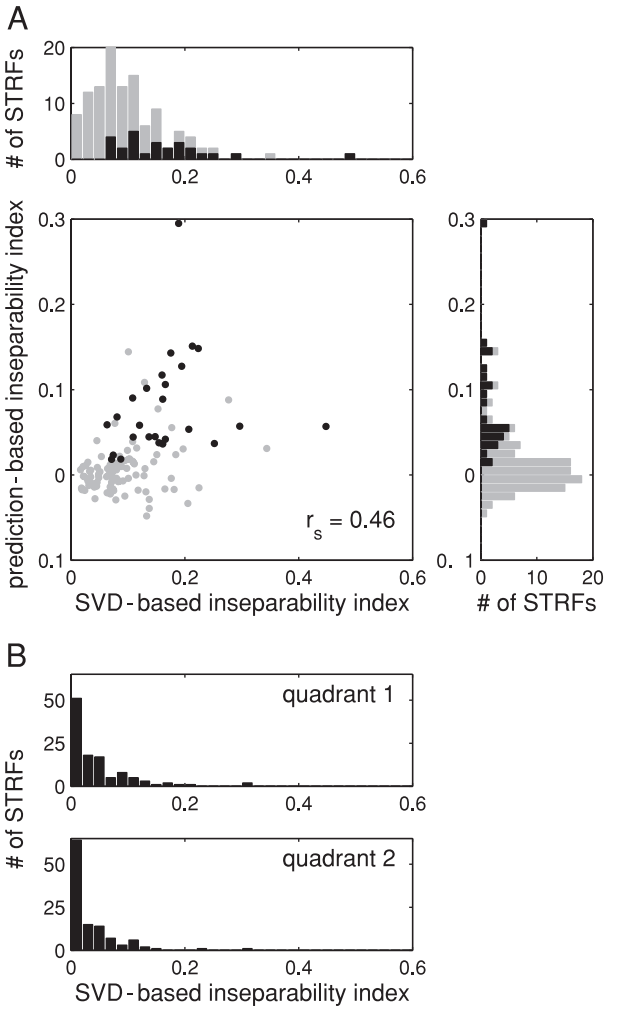

FIG. 10. Spectrotemporal separability of STRFs. *A*: population measures of STRF separability. The scatter plot compares 2 different indices of inseparability in STRFs: a measure based on the extent to which neuronal response predictions can be improved using an inseparable rather than a separable model of the STRF, and a measure of spectral concentration in higher components of the singular value decomposition of the STRF matrix (as in Depireux et al. 2001). Histograms along side and the top of the scatter plot are marginal distributions for the prediction-based and SVD-based inseparability indices, respectively. ● and ■, STRFs for which the prediction-based inseparability index was significantly greater than 0 (i.e., significantly inseparable STRFs). The Spearman rank correlation coefficient is indicated and was significant. Note that a sizeable minority of the STRFs were significantly inseparable according to the prediction-based inseparability test and that the values of the SVD-based inseparability index for these STRFs were often low (0.06–0.45). *B*: population measures of quadrant separability, after Depireux et al. (2001). Separability was quantified for the 1st and 2nd quadrants of the 2-dimensional Fourier transform of the STRF, using the SVD-based inseparability measure from *A*. *Top*: the distribution of this SVD-based inseparability index for the first quadrant, which would include representations of ripple stimuli whose spectral envelopes moved downward in frequency over time (Depireux et al. 2001). *Bottom*: the distribution for the 2nd quadrant, which would include representations of upward moving ripple stimuli. Note that the distributions are strongly peaked at 0, suggesting that the STRFs tend to be quadrant separable.

indices were significantly correlated across the population (2-tailed Spearman rank correlation test, $r_s = 0.46$, $P < 0.0001$). Note, however, that values of the SVD-based inseparability index were quite low even for STRFs with significantly inseparable STRFs according to the prediction-based measure. [Quantitatively similar results were obtained even when the SVD-based measure was defined relative to only the first 3 singular values of the SVD, as in Sen et al. (2001)]. For further comparison with previous studies, Fig. 10*B* shows the distribution of the SVD-based inseparability index applied to the first and second quadrants of the two-dimensional Fourier transform of each STRF; the strong peak near zero in both distributions suggests that STRFs in mouse auditory cortex tend to be "quadrant separable" (Depireux et al. 2001).

Responses to tonal stimuli

The major findings of the STRF analysis regarding the structure of receptive fields in AI and AAF were confirmed by analysis of multi-unit responses to tonal stimuli. Figure 11 displays smoothed frequency-intensity tuning curves and cumulative PSTHs for responses to tonal stimuli at the same AI and AAF recording sites that produced the STRFs depicted in Fig. 5, *A* and *B*. To facilitate comparison of the frequency-intensity tuning curves and STRFs, solid lines along the top of each plot show the frequency tuning curve averaged over the 25- to 70-dB SPL intensity range spanned by tone pips in the dynamic random chord stimulus, and dashed lines show the spectral profile for the corresponding STRF from Fig. 5. Like their corresponding STRFs, the tuning curves from these AI and AAF sites had similar spectral tuning, with maximum sensitivity to sounds in the 10- to 16-kHz frequency range and comparable response bandwidths. However, the PSTHs at the two recording sites were very different; both first-spike latency and response duration were longer for the AI than for the AAF site. The longer response duration at the AI site arose not simply from wider variation in response latency for tones of different frequencies, but from more prolonged responses to individual tone bursts (not shown). Thus these AI and AAF responses to tonal stimuli, like the corresponding STRFs for the same recording sites, appeared to be quite different in temporal structure despite their similar spectral characteristics.

Results for the entire population of AI and AAF recording sites are illustrated in Fig. 12. As shown in Fig. 12*A*, the distribution of first-spike latencies for AI sites was significantly shifted toward longer values relative to the distribution for AAF sites (1-tailed K-S test, $P < 0.0001$, $D_{66} = 0.55$). Moreover, although the very shortest response latencies recorded in the two fields were similar (5–6 ms), the mean first-spike latency for AI was longer than the mean latency for AAF (mean ± SE, 17 ± 1 ms for AI and 11 ± 1 ms for AAF; 1-tailed *t*-test, $P < 0.0001$, $t_{64} = 4.28$). Likewise, although AI and AAF response durations spanned a similar range (Fig. 12*B*), the distribution was significantly shifted toward longer durations for AI than AAF (1-tailed K-S test, $P < 0.005$, $D_{66} = 0.42$), and the mean of the AI distribution was 20 ms longer than the mean of the AAF distribution (59 ± 4 ms for AI, 39 ± 3 ms for AAF; 1-tailed *t*-test, $P < 0.0001$, $t_{64} = 4.24$). (Similar results were obtained when response duration was measured only for stimuli with frequencies near the CF and amplitudes near threshold; see METHODS.) In contrast, normalized bandwidths at 10 dB above threshold were very broad in both AI and AAF (Fig. 12*C*) with no significant difference observed between the AI and AAF distributions (2-tailed K-S test, $P > 0.8$) or between the distribution means (0.48 ± 0.03 for AI, 0.54 ± 0.05 for AAF; 2-tailed *t*-test, $P > 0.3$). No significant correlations were observed between any of these response measures, except for a correlation between response duration

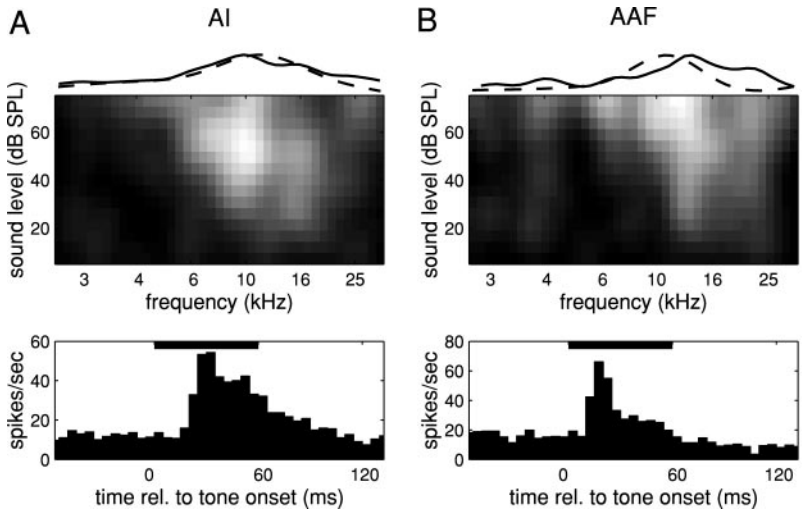

FIG. 11. Examples of responses to tonal stimuli taken from the same recording sites that produced the STRFs shown in Fig. 5, *A* and *B*. Solid curves (*top*) indicate the frequency tuning of responses to tonal stimuli within the 25- to 70-dB SPL intensity range spanned by the dynamic random chord stimulus; dashed curves display spectral profiles for the corresponding STRFs from Fig. 5, scaled to facilitate comparison. Frequency-intensity tuning curves (*top panels*) show firing rate as function of both tone frequency and sound level, with lighter regions representing higher neuronal firing rates. Frequency-intensity tuning curves and frequency tuning curves were smoothed for display with a Gaussian of SD 1.5 bins. Cumulative poststimulus time histograms (*bottom panels*) display firing rate in 5-ms bins, summed over all stimuli used to construct the tuning curves. The black bar above each poststimulus time histogram (PSTH) indicates the duration of the tone burst (cosine gating with 5-ms rise/fall time not shown). *A*: AI recording site. *B*: AAF site. Note that the tuning curves at the AI and AAF sites appear similar, but the PSTHs are quite different; both first-spike latency and response duration were longer at the AI site. Also note that the frequency tuning is similar to that observed in the STRFs obtained from the same sites (Fig. 5, *A* and *B*).

and normalized BW10 for AAF recording sites (2-tailed Spearman rank correlation test, $r_s = 0.53$, $P < 0.005$).

Overall these findings corroborate the results of the STRF analysis by demonstrating that temporal properties of auditory responses were longer on average in AI than in AAF and that the frequency tuning of the responses in both areas was very broad. Indeed, recording site by recording site, there were significant positive correlations between traditional measures of responses to tonal stimuli and STRF measures derived from responses to dynamic random chord stimuli. As illustrated in Fig. 13, characteristic frequencies of frequency-intensity tuning curves were correlated with peak frequencies of STRFs (Fig. 13*A*; 2-tailed Spearman rank correlation test, $r_s = 0.65$, $P < 0.0001$); first-spike latencies for responses to tonal stimuli were correlated with STRF peak latencies (Fig. 13*B*; $r_s = 0.66$, $P < 0.0001$); normalized BW10s for tuning curves were correlated with normalized STRF bandwidths (Fig. 13*C*; $r_s = 0.46$, $P < 0.005$); and the durations of responses to tonal stimuli were correlated with excitatory subfield durations for STRFs (Fig. 13*D*; $r_s = 0.33$, $P < 0.005$). These correlations suggest strong analogies between traditional receptive-field measures based on responses to tonal stimuli and STRF measures based on responses to dynamic random chord stimuli.

DISCUSSION

We have shown that the temporal properties of auditory receptive fields in mouse AI and AAF differ; peak latency and receptive-field duration (measured from STRFs) and first-spike latency and response duration (measured from responses to tonal stimuli) were all significantly longer in AI than in AAF, although the earliest response latencies and the range of receptive-field and response durations were similar in the two areas. Spectrally, AI and AAF responses tended to be broad, with similar bandwidths for responses to tonal stimuli and slightly larger bandwidths in AI than in AAF for STRFs computed from responses to dynamic random chord stimuli. Ultrasound responses were also evident in both areas at recording sites that showed tonotopically appropriate sensitivities at lower frequencies. Finally, nearly one-quarter of the STRFs in both AI and AAF had significantly inseparable spectrotemporal structure, which usually took the form of clearly disjoint excitatory and inhibitory subfields or a pronounced spectrotemporal slant in the receptive field. These results provide the first detailed description of auditory receptive-field properties in the mouse and demonstrate that mouse auditory responses can be spectrotemporally complex. The data also suggest that although neuronal response characteristics in AI and AAF are quite similar overall, area AAF may be specialized for faster temporal processing than area AI. In this section, we consider each of the major results in the context of previous work in other species, and then discuss the relative contributions of the two different types of receptive-field analysis that have been applied together here.

Temporal differences between AI and AAF

The finding that auditory responses in area AI generally have longer latencies and durations than responses in area AAF may at first seem surprising, because areas dubbed "primary sensory" fields are usually thought to be those with the fastest responses. The anatomical connections of areas AI and AAF in the mouse have not been compared in detail, so there is as yet no definitive anatomical evidence to support the parcellation of auditory fields described by Stiebler et al. (1997) [except for UF; see Hofstetter and Ehret (1992)]. Therefore one possible explanation for the observed pattern of temporal differences is that area "AAF" is actually true primary auditory cortex and area "AI" a secondary but tonotopic posterior auditory field.

This possibility, although it cannot yet be ruled out, seems unlikely for two reasons. First, although first-spike latencies are significantly longer on average in AI than in AAF, the *earliest* response latencies in the two areas are similar. Thus there is evidence to suggest that areas AI and AAF in the mouse receive concurrent thalamic input, as do areas AI and AAF in other species (Andersen et al. 1980; Budinger et al. 2000; Imaizumi et al. 2002; Winer 1992). Second, previous studies in cat and ferret support the hypothesis that area AAF may be specialized for faster temporal processing than AI. Response latencies have been reported to be shorter in AAF than AI in recent studies of both cat (Eggermont 1998) and ferret (Kowalski et al. 1995) auditory cortex as we have now shown for mouse auditory cortex. Investigations of cat auditory cortex have also demonstrated that AAF neurons

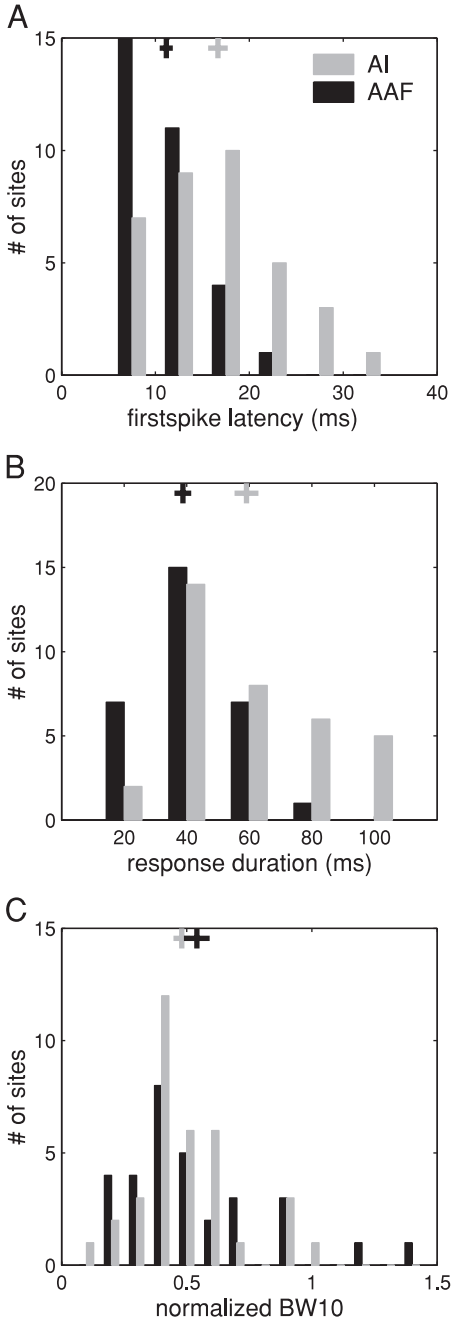

FIG. 12. Temporal and spectral properties of responses to tonal stimuli. Conventions as in Figs. 6 and 7. *A*: first-spike latencies. *B*: response durations. *C*: bandwidths at 10 dB above threshold, normalized by characteristic frequency. Note that first-spike latencies and response durations were significantly longer at AI than at AAF recording sites, while bandwidths in the 2 auditory fields were similar.

can follow significantly faster temporal modulations than AI neurons (Schreiner and Urbas 1988); this result is consistent with the observation of shorter receptive-field and response durations in mouse AAF than in mouse AI. Therefore we conclude that the assignment of auditory areas outlined by Stiebler et al. (1997) is most likely correct and that area AAF in the mouse, like area AAF in other species, may be more capable of fast temporal processing than area AI. It is also possible that the temporal processing capabilities of AAF were especially obvious in these experiments because the recordings were all obtained from the left hemisphere; the left hemisphere appears to be specialized for auditory temporal processing in rodents (Fitch et al. 1993) as well as in humans (Zatorre and Belin 2001).

Spectral similarity of AI and AAF

Neurons in mouse AI and AAF share a similar range of receptive-field bandwidths as measured from tuning curves constructed from responses to tonal stimuli. This finding is consistent with the conclusions of comparable studies of auditory receptive fields in AI and AAF of gerbil (Redies et al. 1989; Thomas et al. 1993) and cat (Knight 1977; Phillips and Irvine 1982), although bandwidths have been reported to be larger in AAF than in AI of ferret (Kowalski et al. 1995). Analysis of STRFs derived from responses to dynamic random chord stimuli revealed slightly larger STRF bandwidths in AI than in AAF. No previous results from other species are directly comparable in this case because bandwidths in AI and AAF have not been compared in other animals using STRFs or broadband stimuli. However, previous studies do suggest that response bandwidth measures may differ depending on the bandwidth of the stimulus used to evoke the neuronal response (Brugge et al. 1998; Calhoun and Schreiner 1998; Ehret and Schreiner 2000; Schreiner and Mendelson 1990) and therefore that responses to tonal stimuli and dynamic random chord stimuli might be expected to have subtly different spectral characteristics (see *Responses to complex versus tonal stimuli*).

The absolute magnitudes of response bandwidths in mouse AI and AAF seem to resemble those in primary auditory cortex of other rodents (Kilgard and Merzenich 1999; Redies et al. 1989; Sally and Kelly 1988; Thomas et al. 1993) but appear broader on average than auditory receptive-field bandwidths in the ferret (Kowalski et al. 1995; Phillips et al. 1988), cat (Schreiner and Mendelson 1990; Sutter and Schreiner 1995), and monkey (Cheung et al. 2001; Recanzone et al. 1999). The relatively broad frequency tuning observed in mouse auditory cortex might therefore be a feature of all rodent auditory receptive fields or perhaps even a general characteristic of auditory responses in animals for which avoiding predators is a more common activity than hunting prey.

The observation that some neurons in mouse AI and AAF show ultrasound sensitivity is also consistent with previous studies; Stiebler et al. (1997) reported responses with both low-frequency and ultrasound peaks in AI and AAF near the borders with UF. In the present experiments, we did only a sparse mapping of the auditory cortex, to reserve sufficient time for detailed characterization of neuronal responses at likely AI and AAF sites. Therefore it is possible that our recordings that showed ultrasound sensitivity were also on the borders of the ultrasound field UF and that the electrodes picked up activity from neurons in that field. If so, however, the borders dividing UF, AI, and AAF are very indistinct. Ultrasound sensitivity was observed in STRFs from single-unit as well as cluster recordings at recording sites showing low-frequency tuning that was clearly tonotopically appropriate to AI or AAF. Moreover, we found sites with ultrasound sensitivity in both AI and AAF, and the topographic organization of mouse auditory cortex makes it very unlikely that AI sites with tuning to frequencies much lower than 40 kHz would be adjacent to neurons in UF. Thus either AI, AAF, and UF

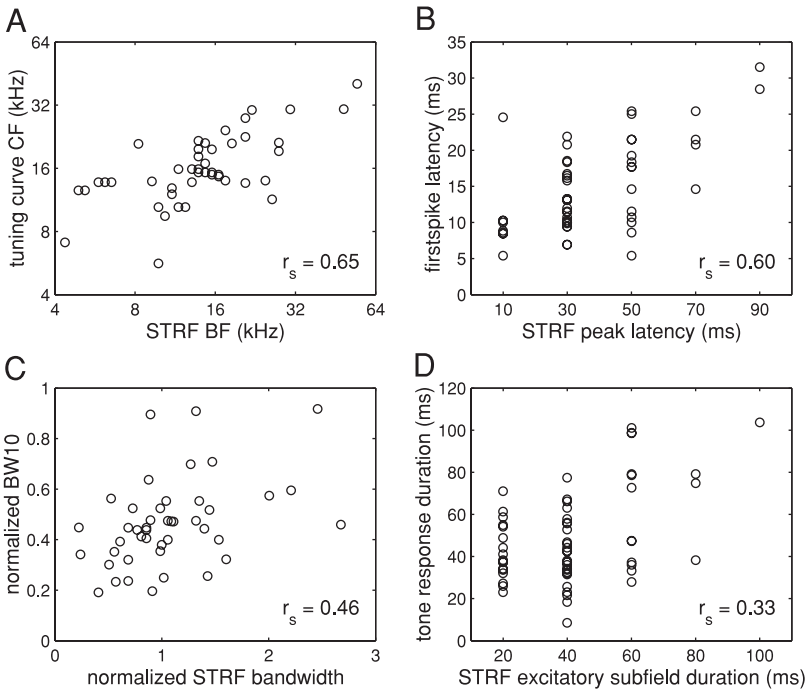

FIG. 13. Correlations between measures of responses to isolated tonal stimuli and related STRF measures derived from responses to dynamic random chord stimuli. Data for AI and AAF sites are pooled to emphasize site-by-site correlations. *A*: tuning curve characteristic frequency vs. STRF best frequency. *B*: first-spike latency from responses to tonal stimuli vs. STRF peak latency. *C*: normalized BW10 from tuning curves vs. normalized STRF bandwidth. *D*: duration of peak response to tonal stimuli vs. STRF excitatory subfield duration. Plots *A* and *C* include only recording sites for which the STRF peak did not fall on the edge of the frequency range. The *x* axis in plots *B* and *D* is coarsely discretized because STRF temporal measures were limited to the 20-ms temporal resolution of the STRF (see METHODS). Spearman rank correlation coefficients are indicated; all correlations were significant.

neurons are extensively intermingled along the borders between the auditory fields or else the observed ultrasound STRFs represent the activity of ultrasound-sensitive AI and AAF neurons rather than UF neurons. The presence of ultrasound sensitivity in AI and AAF may reflect the importance of these high frequencies in mouse communication sounds (Ehret 1992; Haack et al. 1983; Nyby 2001).

Spectrotemporally inseparable responses

Nearly one-quarter of STRFs recorded in both AI and AAF were spectrotemporally inseparable as demonstrated by the fact that an inseparable model of the STRF predicted neuronal responses to novel stimulus segments significantly more accurately than did the best separable model of the STRF. Inseparable spectrotemporal structure in the STRFs usually appeared in the form of disjoint excitatory and inhibitory subfields or a pronounced spectrotemporal slant in the receptive field (e.g., Fig. 9). These inseparable STRFs suggest neuronal selectivity to sound combinations and frequency sweeps, as has been observed in many other species (e.g., deCharms et al. 1998; Mendelson et al. 1993; Nelken and Versnel 2000; Nelken et al. 1994; Orduna et al. 2001; Suga et al. 1979; Tian and Rauschecker 1998). Such STRFs might be specialized for detection of specific sounds with ecological relevance to mice; complex spectrotemporal features are evident in many mouse vocalizations (Ehret and Riecke 2002; Geissler and Ehret 2002; Haack et al. 1983) as well as in other natural sounds (Attias and Schreiner 1997; Nelken et al. 1999).

Previous studies in cat (Miller et al. 2002), ferret (Depireux et al. 2001), and monkey (deCharms et al. 1998) auditory cortex, and additionally in cat inferior colliculus (Qiu et al. 2003) and songbird auditory nuclei (Sen et al. 2001), have also reported some STRFs with complex, clearly inseparable structure. Relative to the STRF populations in some of these previous investigations (e.g., Depireux et al. 2001; Sen et al. 2001), the values of SVD-based inseparability indices for mouse STRFs were quite low; nevertheless, many of these mouse STRFs proved to be significantly inseparable in a test based on the accuracy of neuronal response predictions. The most comprehensive previous studies of spectrotemporal inseparability in STRFs have focused on ferret auditory cortex (Depireux et al. 2001; Kowalski et al. 1996a,b) and have reported that receptive fields in ferret AI are "quadrant separable" (i.e., separable when mapped with spectrally sinusoidal "ripple" stimuli moving in only 1 direction) but not "fully separable" (i.e., separable when mapped with ripple stimuli moving in 2 directions). As shown in Fig. 10, we found that mouse auditory receptive fields also tend to be quadrant separable but not necessarily fully separable. Similar results were obtained in both AI and AAF, suggesting that whatever information processing constraints underlie quadrant separability (Depireux et al. 2001) are shared by both auditory fields.

Responses to complex versus tonal stimuli

There are several reasons why the results of the analysis of responses to tonal stimuli might have been expected to differ from the results of the STRF analysis of responses to dynamic random chord stimuli, even though the data for the two analyses were collected from the same recording sites. First, thresholded multiunit recordings were used for analysis of responses to tonal stimuli, while spike-sorted single-unit or small-cluster recordings of responses to dynamic random chord stimuli were used to derive the STRFs. (Although we found no significant differences between single-unit and cluster recordings in the STRF analysis, the multiunit recordings of responses to tonal stimuli likely included many more neurons than STRF cluster recordings and so might have shown more discrepancies from single-unit data.) Second, there are known to be profound nonlinearities in the responses of auditory cortex neurons to wide- versus narrow-band sounds. In particular, the apparent bandwidth of the receptive field depends in part on the bandwidth of the stimulus used to measure it (Brugge et al. 1998; Calhoun and Schreiner 1998; Ehret and

Schreiner 2000; Schreiner and Mendelson 1990). Finally, as spectrogram-linear approximations to true (nonlinear) receptive fields, STRFs are limited even in their description of responses to dynamic random chord stimuli. In fact, we have shown elsewhere that linear STRFs account for no more than half of the stimulus-dependent variability in neuronal responses to dynamic random chord stimuli (Sahani and Linden 2003b); this finding holds true for the STRFs considered here as well as for STRFs from rat auditory cortex.

With these considerations in mind, it is noteworthy that the results of our analysis of responses to tonal stimuli were so consistent with the results of the STRF analysis. The only discrepancy between the two population analyses occurred in the comparison of frequency tuning in AI and AAF; the STRF analysis found that AI STRFs were slightly but significantly broader in bandwidth than AAF STRFs, while the analysis of responses to tonal stimuli found no significant difference between the two auditory fields in normalized bandwidth at 10 dB above threshold. This small divergence in the findings from the two spectral analyses is not surprising given not only that narrow- and broad-band stimuli would be expected to evoke different responses in auditory cortex (Brugge et al. 1998; Calhoun and Schreiner 1998; Schreiner and Mendelson 1990; Ehret and Schreiner 2000; Schreiner and Mendelson 1990) but also that the two bandwidth measures are defined differently with respect to stimulus intensity. Indeed, the consistency in the results of the two analyses is much more striking than this minor difference. Recording site by recording site, STRF measures correlated with related frequency-intensity tuning curve or PSTH measures from the same recording sites. This correlation suggests that the two approaches provide broadly consistent and complementary accounts of receptive-field structure and lend assurance that the first-order approximation inherent in the STRF captures the same receptive-field features extracted by more traditional response measures.

However, despite the similarities, the two analyses also provide different information about receptive-field structure. For example, responses to isolated tone bursts can be used to estimate first-spike latencies, which cannot be determined from responses to a continuous stimulus like the dynamic random chord stimulus. Frequency-intensity tuning curves can be used to examine response properties such as bandwidth as a function of intensity, whereas examination of intensity-dependent properties is considerably more difficult (although theoretically possible) in analysis of STRFs. Conversely, the STRF analyses simplify examination of the inhibitory subregions of receptive fields, which are difficult to characterize in low-firing auditory neurons using isolated tone bursts. Most importantly, however, STRFs provide information about the incidence and form of spectrotemporally inseparable receptive fields, information that cannot be extracted from responses to isolated tonal stimuli. The two types of analysis applied here therefore produced not only consistent but also complementary results, with the STRF analysis providing the added benefit of information about complex structure in auditory receptive fields. The first-order descriptions of responses provided by both of these analysis methods have demonstrated that mouse AI and AAF receptive fields differ in their temporal properties and can display complex spectrotemporal structure. Given this complexity of some mouse receptive fields, and the known limitations of both traditional analysis methods and linear STRF analysis, the obvious remaining challenge is to move beyond these first-order descriptions to a more complete account of mouse auditory receptive fields that includes nonlinear properties of neuronal responses.

We thank G. Ehret for advice on surgical and recording procedures, M. Kvale for helpful comments on the manuscript and for the use of spike-sorting user interface software, and B. Bonham for the use of frequency-intensity tuning curve analysis software. J. F. Linden collected and analyzed the data and wrote the manuscript; R. C. Liu helped with experimental procedures; M. Sahani developed the STRF estimation and analysis methods, including the novel separability analysis; and C. E. Schreiner and M. M. Merzenich assisted with experimental design and interpretation of results.

DISCLOSURES

This work was supported by National Institutes of Health Grants DC-00399, DC-05279, DC-02260, and NS-10414; the Sloan and Swartz Foundations; and the Gatsby Trust.

REFERENCES

Aertsen AMHJ and Johannesma PIM. The spectro-temporal receptive field: a functional characteristic of auditory neurons. *Biol Cybern* 42: 133–143, 1981.

Andersen RA, Knight PL, and Merzenich MM. The thalamocortical and corticocortical connections of AI, AII, and the anterior auditory field (AAF) in the cat: evidence for two largely segregated systems of connections. *J Comp Neurol* 194: 663–701, 1980.

Attias H and Schreiner CE. Low-order temporal statistics of natural sounds. In: *Advances in Neural Information Processing Systems*, edited by Mozer MC, Jordan MI, and Petsche T. Cambridge, MA: MIT Press, 1997, vol. 9, p. 27–33.

Battey JF Jr. Human hereditary hearing impairment: research progress fueled by the human genome project and mouse models. In: *Handbook of Mouse Auditory Research: From Behavior to Molecular Biology*, edited by Willott JF. Boca Raton, FL: CRC, 2001, chapt. 26, p. 391–400.

Brugge JF, Reale RA, and Hind JE. Spatial receptive fields of primary auditory cortical neurons in quiet and in the presence of continuous background noise. *J Neurophysiol* 80: 2417–2432, 1998.

Budinger E, Heil P, and Scheich H. Functional organization of auditory cortex in the Mongolian gerbil (*Meriones unguiculatus*). IV. Connections with anatomically characterized subcortical structures. *Eur J Neurosci* 12: 2452–2474, 2000.

Calhoun BM and Schreiner CE. Spectral envelope coding in cat primary auditory cortex: linear and non-linear effects of stimulus characteristics. *Eur J Neurosci* 10: 926–940, 1998.

Cheung SW, Bedenbaugh PH, Nagarajan SS, and Schreiner CE. Functional organization of squirrel monkey primary auditory cortex: responses to pure tones. *J Neurophysiol* 85: 1732–1749, 2001.

deCharms RC, Blake DT, and Merzenich MM. Optimizing sound features for cortical neurons. *Science* 280: 1439–1443, 1998.

Depireux DA, Simon JZ, Klein DJ, and Shamma SA. Spectro-temporal response field characterization with dynamic ripples in ferret primary auditory cortex. *J Neurophysiol* 85: 1220–1234, 2001.

Duda RO and Hart PE. *Pattern Classification and Scene Analysis.* New York: Wiley, 1973.

Eggermont JJ. Representation of spectral and temporal sound features in three cortical fields of the cat. Similarities outweigh differences. *J Neurophysiol* 80: 2743–2764, 1998.

Eggermont JJ, Aertsen AM, and Johannesma PI. Quantitative characterisation procedure for auditory neurons based on the spectro-temporal receptive field. *Hear Res* 10: 167–190, 1983a.

Eggermont JJ, Johannesma PM, and Aertsen AM. Reverse-correlation methods in auditory research. *Q Rev Biophys* 16: 341–414, 1983b.

Ehret G. Categorical perception of mouse-pup ultrasounds in the temporal domain. *Anim Behav* 43: 409–416, 1992.

Ehret G and Riecke S. Mice and humans perceive multiharmonic communication sounds in the same way. *Proc Natl Acad Sci USA* 99: 479–482, 2002.

Ehret G and Schreiner CE. Regional variations of noise-induced changes in operating range in cat AI. *Hear Res* 141: 107–116, 2000.

Escabi MA and Schreiner CE. Nonlinear spectrotemporal sound analysis by neurons in the auditory midbrain. *J Neurosci* 22: 4114–4131, 2002.

Fitch RH, Brown CP, O'Connor K, and Tallal P. Functional lateralization for auditory temporal processing in male and female rats. *Behav Neurosci* 107: 844–850, 1993.

Geissler DB and Ehret G. Time-critical integration of formants for perception of communication calls in mice. *Proc Natl Acad Sci USA* 99: 9021–9025, 2002.

Haack B, Markl H, and Ehret G. Sound communication between parents and offspring. In: *The Auditory Psychobiology of the Mouse*, edited by Willott JF. Springfield, IL: Thomas, 1983, chapt. 2, p. 57–97.

Henry KR and McGinn MD. The mouse as a model for human audition: a review of the literature. *Audiology* 31: 181–189, 1992.

Hofstetter KM and Ehret G. The auditory cortex of the mouse: connections of the ultrasonic field. *J Comp Neurol* 323: 370–386, 1992.

Imaizumi K, Schreiner CE, Winer JA, and Lee CC. Parallel processing in two tonotopic areas of cat auditory cortex. *Soc Neuroci Abstr* 32: 458.15, 2002.

Keller CH and Takahashi TT. Representation of temporal features of complex sounds by the discharge patterns of neurons in the owl's inferior colliculus. *J Neurophysiol* 84: 2638–2650, 2000.

Kilgard MP and Merzenich MM. Distributed representation of spectral and temporal information in rat primary auditory cortex. *Hear Res* 134: 16–28, 1999.

Kisley MA and Gerstein GL. Trial-to-trial variability and state-dependent modulation of auditory-evoked responses in cortex. *J Neurosci* 19: 10451–10460, 1999.

Knight PL. Representation of the cochlea within the anterior auditory field (AAF) of the cat. *Brain Res* 130: 447–467, 1977.

Kowalski N, Depireux DA, and Shamma SA. Analysis of dynamic spectra in ferret primary auditory cortex. I. Characteristics of single-unit responses to moving ripple spectra. *J Neurophysiol* 76: 3503–3523, 1996a.

Kowalski N, Depireux DA, and Shamma SA. Analysis of dynamic spectra in ferret primary auditory cortex. II. Prediction of unit responses to arbitrary dynamic spectra. *J Neurophysiol* 76: 3524–3534, 1996b.

Kowalski N, Versnel H, and Shamma SA. Comparison of responses in the anterior and primary auditory fields of the ferret cortex. *J Neurophysiol* 73: 1513–1523, 1995.

Lewicki MS. Bayesian modeling and classification of neural signals. *Neural Comput* 6: 1005–1030, 1994.

Lindgren BW. *Statistical Theory*. Boca Raton, FL: Chapman and Hall/CRC, 1993.

McHugh TJ, Blum KI, Tsien JZ, Tonegawa S, and Wilson MA. Impaired hippocampal representation of space in CA1-specific NMDAR1 knockout mice. *Cell* 87: 1339–1349, 1996.

Mendelson JR, Schreiner CE, Sutter ML, and Grasse KL. Functional topography of cat primary auditory cortex: responses to frequency-modulated sweeps. *Exp Brain Res* 94: 65–87, 1993.

Miller LM, Escabí MA, Read HL, and Schreiner CE. Functional convergence of response properties in the auditory thalamocortical system. *Neuron* 32: 151–160, 2001.

Miller LM, Escabí MA, Read HL, and Schreiner CE. Spectrotemporal receptive fields in the lemniscal auditory thalamus and cortex. *J Neurophysiol* 87: 516–527, 2002.

Nelken I, Prut Y, Vaadia E, and Abeles M. Population responses to multifrequency sounds in the cat auditory cortex: one- and two-parameter families of sounds. *Hear Res* 72: 206–22, 1994.

Nelken I, Rotman Y, and Bar Yosef O. Responses of auditory-cortex neurons to structural features of natural sounds. *Nature* 397: 154–157, 1999.

Nelken I and Versnel H. Responses to linear and logarithmic frequency-modulated sweeps in ferret primary auditory cortex. *Eur J Neurosci* 12: 549–562, 2000.

Nirenberg S and Cepko C. Targeted ablation of diverse cell classes in the nervous system in vivo. *J Neurosci* 13: 3238–3251, 1993.

Nyby JG. Auditory communication among adults. In: *Handbook of Mouse Auditory Research: From Behavior to Molecular Biology*, edited by Willott JF. Boca Raton, FL: CRC, 2001, chapt. 1, p. 3–18.

Orduña I, Mercado E III, Gluck MA, and Merzenich MM. Spectrotemporal sensitivities in rat auditory cortical neurons. *Hear Res* 160: 47–57, 2001.

Phillips DP and Irvine DR. Properties of single neurons in the anterior auditory field (AAF) of cat cerebral cortex. *Brain Res* 248: 237–244, 1982.

Phillips DP, Judge PW, and Kelly JB. Primary auditory cortex in the ferret (*Mustela putorius*): neural response properties and topographic organization. *Brain Res* 443: 281–294, 1988.

Qiu A, Schreiner CE, and Escabi MA. Gabor analysis of auditory midbrain receptive fields: spectro-temporal and binaural composition. *J Neurophysiol* 89: 456–476, 2003.

Recanzone GH, Schreiner CE, Sutter ML, Beitel RE, and Merzenich MM. Functional organization of spectral receptive fields in the primary auditory cortex of the owl monkey. *J Comp Neurol* 415: 460–481, 1999.

Redies H, Sieben U, and Creutzfeldt OD. Functional subdivisions in the auditory cortex of the guinea pig. *J Comp Neurol* 282: 473–488, 1989.

Rutkowski RG, Shackleton TM, Schnupp JW, Wallace MN, and Palmer AR. Spectrotemporal receptive field properties of single units in the primary, dorsocaudal and ventrorostral auditory cortex of the guinea pig. *Audiol Neurootol* 7: 214–217, 2002.

Sahani M and Linden JF. Evidence optimization techniques for estimating stimulus-response functions. In: *Advances in Neural Information Processing Systems*, edited by Becker S, Thrun S, and Obermeyer K. Cambridge, MA: MIT Press, 2003a, vol. 15, p. 301–308. Available online via http://www.nips.cc/Proceedings/.

Sahani M and Linden JF. How linear are auditory cortical responses? In: *Advances in Neural Information Processing Systems*, edited by Becker S, Thrun S, and Obermeyer K. Cambridge, MA: MIT Press, 2003b, vol. 15, p. 109–116. Available online via http://www.nips.cc/Proceedings/.

Sally SL and Kelly JB. Organization of auditory cortex in the albino rat: sound frequency. *J Neurophysiol* 59: 1627–1638, 1988.

Schnupp JW, Mrsic-Flogel TD, and King AJ. Linear processing of spatial cues in primary auditory cortex. *Nature* 414: 200–204, 2001.

Schreiner CE and Mendelson JR. Functional topography of cat primary auditory cortex: distribution of integrated excitation. *J Neurophysiol* 64: 1442–1459, 1990.

Schreiner CE and Urbas JV. Representation of amplitude modulation in the audiory cortex of the cat. II. Comparison between cortical fields. *Hear Res* 32: 49–63, 1988.

Sen K, Theunissen FE, and Doupe AJ. Feature analysis of natural sounds in the songbird auditory forebrain. *J Neurophysiol* 86: 1445–1458, 2001.

Shen JX, Xu ZM, and Yao YD. Evidence for columnar organization in the auditory cortex of the mouse. *Hear Res* 137: 174–177, 1999.

Smith PH and Populin LC. Fundamental differences between the thalamocortical recipient layers of the cat auditory and visual cortices. *J Comp Neurol* 436: 508–519, 2001.

Stiebler I, Neulist R, Fichtel I, and Ehret G. The auditory cortex of the house mouse: left-right differences, tonotopic organization and quantitative analysis of frequency representation. *J Comp Physiol [A]* 181: 559–571, 1997.

Suga N, O'Neill WE, and Manabe T. Harmonic-sensitive neurons in the auditory cortex of the mustache bat. *Science* 203: 270–274, 1979.

Sutter ML and Schreiner CE. Topography of intensity tuning in cat primary auditory cortex: single-neuron versus multiple-neuron recordings. *J Neurophysiol* 73: 190–204, 1995.

Theunissen FE, David SV, Singh NC, Hsu A, Vinje WE, and Gallant JL. Estimating spatio-temporal receptive fields of auditory and visual neurons from their responses to natural stimuli. *Network* 12: 289–316, 2001.

Theunissen FE, Sen K, and Doupe AJ. Spectral-temporal receptive fields of nonlinear auditory neurons obtained using natural sounds. *J Neurosci* 20: 2315–2331, 2000.

Thomas H, Tillein J, Heil P, and Scheich H. Functional organization of auditory cortex in the Mongolian gerbil (*Meriones unguiculatus*). I. Electrophysiological mapping of frequency representation and distinction of fields. *Eur J Neurosci* 5: 882–897, 1993.

Tian B and Rauschecker JP. Processing of frequency-modulated sounds in the cat's posterior auditory field. *J Neurophysiol* 79: 2629–2642, 1998.

Tolhurst DJ, Movshon JA, and Dean AF. The statistical reliability of signals in single neurons in cat and monkey visual cortex. *Vision Res* 23: 775–785, 1983.

Willott JF (editor). *Handbook of Mouse Auditory Research: From Behavior to Molecular Biology*. Boca Raton, FL: CRC, 2001.

Willott JF, Aitkin LM, and McFadden SL. Plasticity of auditory cortex associated with sensorineural hearing loss in adult C57BL/6J mice. *J Comp Neurol* 329: 402–411, 1993.

Willott JF, Turner JG, and Sundin VS. Effects of exposure to an augmented acoustic environment on auditory function in mice: roles of hearing loss and age during treatment. *Hear Res* 142: 79–88, 2000.

Winer JA. The functional architecture of the medial geniculate body and the primary auditory cortex. In: *The Mammalian Auditory Pathway: Neuroanatomy*, edited by Webster DB, Popper AN, and Fay RR. New York: Springer-Verlag, 1992, p. 222–409.

Zar JH. *Biostatistical Analysis* (3rd ed.). Upper Saddle River, NJ: Prentice-Hall, 1996.

Zatorre RJ and Belin P. Spectral and temporal processing in human auditory cortex. *Cereb Cortex* 11: 946–953, 2001.

Zheng QY, Johnson KR, and Erway LC. Assessment of hearing in 80 inbred strains of mice by ABR threshold analyses. *Hear Res* 130: 94–107, 1999.